RM L51J09

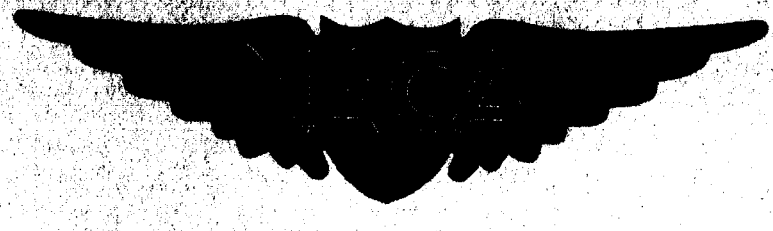

RESEARCH MEMORANDUM

AN INVESTIGATION OF THE AERODYNAMIC CHARACTERISTICS OF A SERIES OF CONE-CYLINDER CONFIGURATIONS AT A MACH NUMBER OF 6.86

By Ralph D. Cooper and Raymond A. Robinson

Langley Aeronautical Laboratory
Langley Field, Va.

NATIONAL ADVISORY COMMITTEE FOR AERONAUTICS

WASHINGTON

December 17, 1951
Declassified January 30, 1959

NATIONAL ADVISORY COMMITTEE FOR AERONAUTICS

RESEARCH MEMORANDUM

AN INVESTIGATION OF THE AERODYNAMIC CHARACTERISTICS OF A SERIES OF CONE-CYLINDER CONFIGURATIONS AT A MACH NUMBER OF 6.86

By Ralph D. Cooper and Raymond A. Robinson

SUMMARY

The results of pressure-distribution and force tests of two series of cone-cylinder configurations in the Langley 11-inch hypersonic tunnel at a Mach number of 6.86 and a Reynolds number of 290,000 based on maximum diameter are presented and compared with theoretical calculations. The first series consisted of three configurations, all of which had 20° conical noses and cylindrical afterbodies with lengths equal to 0, 2, and 4 diameters. The second series consisted of models having cylindrical afterbodies of length equal to 4 diameters and conical noses with apex angles varying from 10° to 180°.

Pressure distributions on the longest 20° cone-cylinder configuration were obtained at four representative angles of attack, 0°, 6.7°, 14°, and 20°. In the axially symmetric case (zero angle of attack) experimental results were in very good agreement with theoretical calculations based on the Taylor-Maccoll theory for the conical portion and on the method of characteristics for the cylindrical portion. At the low angles of attack, experimental pressures on the conical nose were in satisfactory agreement with results calculated according to the conical-flow theories of Stone and Ferri. On the conical nose at the higher angles of attack and on the cylindrical afterbody throughout the angle-of-attack range the hypersonic approximation of Grimminger, Williams, and Young satisfactorily predicts the pressure distributions on the windward side where the theory is applicable. Pressure distributions on the cylindrical afterbody can also be satisfactorily approximated, when the conical-flow solution is known, by extending this solution through a two-dimensional expansion to the cylindrical surface.

Force tests of the three configurations of the first series were made at angles of attack ranging from 0° to approximately 25°. Comparisons between experiment and theory show that the drag at low angles of attack is accurately predicted by Ferri's theory while the lift is

predicted with slightly less accuracy. The hypersonic approximation of Grimminger, Williams, and Young gives accurate drag results throughout the angle-of-attack range; however, the lift, and consequently the lift-drag ratio, are slightly overestimated by this approximate theory. As indicated by theory, the addition of the cylindrical afterbody to the conical nose resulted in a significant increase in the lift-drag ratio of the configuration.

The tests of the second series of configurations, that is, those with varying conical apex angles in the axially symmetric attitude, showed that the results of the Taylor-Maccoll theory agreed with the experimental drag coefficients.

INTRODUCTION

Until very recently it has been necessary to use the results of theoretical studies of the aerodynamic performance of various configurations at high supersonic, or hypersonic, speeds without experimental verification. Therefore, after the completion of the calibration of the flow in a two-dimensional, single-step nozzle in the Langley 11-inch hypersonic tunnel (reference 1), a preliminary model-testing program was initiated to obtain experimental data and evaluate theoretical results at a Mach number of 6.86, which is well beyond the range of previous investigations of a similar nature. The first part of the testing program was devoted to the investigation of the aerodynamic characteristics of several square-plan-form wings (reference 2) while the second part, which is the consideration of the present paper, embodied tests of cone-cylinder configurations.

This paper presents the results of an investigation of two series of models. The first series, which consisted of three configurations having 20° conical noses and cylindrical afterbodies with lengths equal to 0, 2, and 4 diameters, was tested in the angle-of-attack range from 0° to about 25°. The second series, which consisted of seven models having cylindrical afterbodies with length equal to 4 diameters and conical noses with apex angles of 10°, 20°, 30°, 45°, 60°, 90°, and 180°, was tested only in the axially symmetric attitude.

The aerodynamic characteristics of all models were determined by force tests. In addition, pressure distributions at several representative angles of attack were obtained for a cone-cylinder configuration having a 20° apex angle and a 4-diameter afterbody length.

In order to evaluate the relative accuracy and the range of application of the various theories for the flow over cones and cone-cylinders, the results of these tests were compared with calculations from the cone

theory of Ferri (reference 3) and from the cone theory of Stone (reference 4) as tabulated by Kopal (reference 5); also, the hypersonic approximation of Grimminger, Williams, and Young (reference 6) and the hypersonic approximation of Ivey and Morrissette (reference 7). For the axially symmetric case the results from the models with varying apex angles were compared with results from the exact cone theory of Taylor and Maccoll (reference 8).

SYMBOLS

A	area of base of cone or cone-cylinder
C_D	drag coefficient $\left(D/q_1 A\right)$
C_L	lift coefficient $\left(L/q_1 A\right)$
C_m	pitching-moment coefficient measured about cone tip $\left(\frac{\text{Pitching moment}}{q_1 A l_t}\right)$
c_n	local normal-force coefficient normal to body axis
C.P.	distance from tip of cone to center of pressure, body lengths
D	drag
L	lift
M	Mach number
d	maximum diameter of model, 1.17 inches
p	static pressure
q	dynamic pressure
z	distance from apex of cone to axial station
l	length of cylindrical afterbody
l_t	total length of model
α	angle of attack between wind and body axes
β	radial angle about body axis measured from top of body

β' radial angle referred to wind axis

θ included apex angle of cone

Subscripts

b base

c cone or conical nose

cy cylindrical afterbody

max maximum

l free stream

APPARATUS

Wind Tunnel

The Langley 11-inch hypersonic tunnel in which the tests were conducted is of the intermittent-operation type, utilizing both a high-pressure and a vacuum tank. This tunnel is equipped with a two-dimensional, single-step nozzle which produces sufficiently uniform flow for model testing at $M = 6.86$ in an approximately 5-inch-square central core of the test section. A small variation of Mach number with time, observed in calibration tests of this nozzle, was taken into consideration in the reduction of the data obtained in the present tests. A detailed description of the tunnel and the nozzle calibration can be found in references 1 and 9, respectively.

Models

The first series of models, which is shown in figure 1, consisted of three configurations, all having identical conical noses with apex angles of 20° but with cylindrical afterbodies of lengths equal to 0, 2, and 4 body diameters. The maximum total-configuration length was fixed at 8 inches in order to retain the model completely within the uniform flow region of the test section during the high angle-of-attack tests. In order to obtain reasonably large forces which could be measured by existing strain-gage force balances, relatively low fineness ratios were selected. A body diameter of 1.17 inches was used for all configurations tested. Adherence to these considerations resulted in bodies which, despite their low fineness ratios, were quite suitable

for the purposes of checking theoretical calculations and obtaining preliminary experimental design data.

The second series of models, which is shown in figure 2, consisted of seven cone-cylinder configurations having apex angles of 10°, 20°, 30°, 45°, 60°, 90°, and 180° and all having identical cylindrical afterbodies with a length-to-diameter ratio of 4.

An additional model, dimensionally identical to the model of the first series having a conical nose with a 20° apex angle and l/d of 4, was equipped with ten pressure orifices. These orifices were installed along the generatrix of the configuration, five on the conical nose, four on the cylindrical afterbody, and one on the base. The five orifices on the conical surface and the first orifice after the corner on the cylindrical surface were 0.025 inch in diameter; the remaining orifices were 0.040 inch in diameter. These orifices were chosen so that the pressure lag would be as low as possible and the orifices would still be small enough so as not to disturb the flow appreciably. The pressure-test model, together with both the base tube by which it was supported and through which the pressure tubing passed and the mechanism for adjusting the angle of attack, is shown in figure 3. The support from the base of this model was 1/2 inch in diameter and the base orifice was located midway between the side of the support and the side of the cylinder.

All models were machined from steel and had polished surfaces.

Instrumentation

Two strain-gage force balances were used during the course of this investigation. One was employed at moderate and high angles of attack and the other, which was of much greater sensitivity, was used in the low angle-of-attack range (up to about $\alpha = 8^\circ$) where the forces encountered were relatively small. The former was a three-component balance which directly resolved the aerodynamic forces encountered on the model into lift and drag forces. This balance was equipped with a variety of shielded elbow-type adapters which permitted the mounting of models at different angles of attack. Unfortunately, the scatter of the data obtained with the pitching-moment component was so wide and erratic as to render it unusable. The two elements of the moment-measuring component were located at widely separated positions in the balance and the uneven heating to which they were subjected during the course of a test run resulted in their unsatisfactory performance. The elements of the lift and drag measuring components were considerably closer together and, although they did not entirely escape the adverse heating effects, their accuracy was not seriously impaired thereby. The second balance used, the two-component balance, was designed to be alined with the model axis

so that the forces normal and parallel to the model axis were measured. These force balances are described in greater detail in reference 2.

Pressure measurements were recorded by instruments in which the deflection of a metallic diaphragm is converted into the rotation of a small mirror. A beam of light is reflected from this mirror onto a strip of film moving at constant speed so that the trace thus obtained represents a time history of the pressure. In reference 9 a more complete description of these pressure-recording devices is presented.

To supplement the pressure and force data recorded during the tests, schlieren photographs were obtained for each test. The schlieren system is described in reference 9. Although most of the photographs were taken with an exposure of several microseconds, a few were taken with an exposure of 1/150 second.

TESTING PROCEDURE

During the tests, the tunnel was operated at a stagnation pressure of approximately 25.5 atmospheres and a stagnation temperature of approximately 1200° R. With these operating conditions, the Reynolds number per foot of the stream at the test section is 2,930,000 and, consequently, the characteristic Reynolds number referred to the base diameter of the models (d = 1.17 in.) is approximately 290,000. The length of a typical test varied from about 60 to 90 seconds. Since the nozzle was calibrated at 60 seconds from the start of the run, only data obtained at 60 seconds after the start of the test were used, in order to diminish the effects of a small Mach number variation with time.

Except for the case of zero angle of attack, the pressure distribution over the pressure model at a given angle of attack was determined in a series of seven successive runs. For each run in a series, the generatrix containing the pressure orifices was rotated 30° from its previous position while the angle of attack was maintained constant. In this manner, pressure distributions at radial positions corresponding to $\beta = 0^\circ, 30^\circ, 60^\circ, 90^\circ, 120^\circ, 150^\circ$, and 180° were obtained for the three angles of attack, $\alpha = 6.7^\circ, 14^\circ$, and 20°.

Force measurements for the models of the first series were obtained at intervals of about 3° or 4° throughout the entire range of α from 0° to approximately 25°.

ACCURACY OF THE DATA

Pressure data were recorded with instruments which are accurate to within about ±0.5 percent of the upper limit of their operating range. Since it was usually not possible to use the instruments in this favorable range, the accuracy of most of the pressure data is restricted to approximately ±1.0 percent.

The absolute error in the determination of the free-stream Mach number in the central portion of the test section is about ±0.04, as is shown by the calibration curves presented in reference 1.

These errors in Mach number and in pressure determination combine to give a possible error of about ±5 percent in the calculation of C_L and C_D from pressure distributions; however, the actual accuracy realized is considerably better, so that ±3 percent is a reasonable estimate of the error.

The two-component balance is accurate to within about ±0.025 pound in normal force and ±0.005 pound in axial force. Since its range was from only 0 to 1 pound in axial force, the use of this balance was limited to angles of attack of approximately 7.5° or less. For larger angles of attack, the three-component balance, accurate to within ±0.1 pound in lift force and ±0.05 pound in drag force, was used. Combining these errors in force measurement with those associated with the determination of free-stream Mach number and pressure yields the possible errors in lift and drag coefficients shown in the following tables:

Two-Component Balance

C_L	Error	C_D	Error
0.05	±0.008	0.10	±0.005
.12	±.010	.15	±.006
.24	±.014	.20	±.008
.36	±.019		

Three-Component Balance

C_L	Error	C_D	Error
0.49	±0.042	0.24	±0.020
.61	±.046	.37	±.027
.85	±.054	.49	±.029
1.22	±.067	.61	±.033

Again, the accuracy realized by the force tests is better than is indicated by the possible-error values, so that errors greater than about one-half of those shown in the preceding tables were seldom encountered.

In addition, the angle of attack at which the force measurements were obtained was determined from schlieren photographs with an accuracy of approximately ±0.2°.

THEORETICAL CONSIDERATIONS

Exact Solution for Axially Symmetric Case

The complete solution for the potential flow field about an infinite cone in an axially symmetric supersonic stream has been determined by Taylor and Maccoll (reference 8) and evaluated and tabulated in great detail by the computing staff of the Massachusetts Institute of Technology (reference 10). The Taylor-Maccoll solution has been used over the conical nose, and the flow field about the cylindrical afterbody has been computed by the method of characteristics for three-dimensional phenomena (reference 11).

Nonlinear Solution for Inclined Cones

Both first- and second-order nonlinear solutions to the problem of supersonic flow about inclined cones have been developed by Stone (reference 4). In the derivation of this work, Stone shows that each of the various parameters of the flow, that is, the three components of velocity, the pressure, and the density, can be represented by a Fourier expansion. Consideration of the boundary conditions of the problem permits a typical flow parameter to be expressed in the form

$$a = \underline{a} + \alpha b_1 \cos \beta' + \alpha^2 (c_0 + c_2 \cos 2\beta')$$

where $\underline{a}$ designates the axially symmetric value of the parameter, α the angle of attack, β' the coordinate angle with respect to the wind axis, and b_1, c_0, and c_2 the appropriate Fourier coefficients. (In the case of the tangential component of the cross flow, the cosines are replaced by sines as dictated by considerations of symmetry.)

As in the case of the Taylor-Maccoll solution for axially symmetric conical flow, the computing staff of M.I.T. under the direction of Kopal has performed much of the numerical calculations required for the application of this theory and the results have been published in two volumes (references 5 and 12). However, the numerical calculations associated with the terms of second order are of such a lengthy and complex nature that at the present time values corresponding to Mach numbers up to 4 only are available; consequently, it was practical to include in this investigation the results of the first-order solution only. The results of this theory are hereinafter referred to as the Stone-Kopal theory.

It may be pointed out that the radial angles β' and β referred to the wind and body axes, respectively, are identical to the first

order in α. Consequently, in the application of this first-order theory it is not necessary to transform from the wind axis, in which the solution is obtained, to the body axis. (However, as the angle of attack approaches the semiapex angle of the cone, the first-order equivalence between the radial angles in the two coordinate systems departs very severely from their exact relationship, indicating that significant results should not be expected from the first-order theory as α approaches $\theta/2$. For a cone with 10° semiapex angle in a flow at $M = 6.86$, this first-order theory applied at angles of attack above 8.5° yields negative pressure ratios on the upper surface.)

Another first-order solution to the problem of supersonic flows about inclined cones has been developed by Ferri (reference 3). Although this solution is very similar to that of Stone, there are two fundamental differences. First, Ferri investigates the entropy distribution in the flow field about the cone. In contrast to the distribution assumed by Stone, which varies throughout the entire flow field behind the shock, Ferri shows that on the surface of the cone the entropy is constant, although it does vary throughout the remainder of the field. To satisfy this condition of constant entropy on the cone surface, the concept of a thin vortical layer at the cone surface through which there is a large entropy gradient was introduced. The second fundamental difference between these theories is that Ferri has used a coordinate system referred to the cone axis in obtaining his solution. Nevertheless, it is of interest to note that the parameters which are necessary for the application of Ferri's theory can be determined from the M.I.T. tabulated results of Stone's theory, if due regard be given to the change in coordinate system.

These theories are used in place of the conventional linearized theories of flow about inclined cones such as that of Tsien (reference 13), since the nature of the linearized solutions restricts their application to cones having semiapex angles smaller than the Mach angle of the undisturbed stream.

Solution for Flow on Cylindrical Afterbody of Cone-Cylinder Configuration at Angles of Attack

When the solution to the problem of flow over an inclined cone is known, a first approximation to the pressure distributions on the cylindrical afterbody of a cone-cylinder configuration at angles of attack can be made by an extension of the conical flow solution. This extension merely requires that the conical flow be given a two-dimensional Prandtl-Meyer expansion equivalent to the semiapex angle of the cone. The assumption is made that the pressure thus obtained will remain constant along the entire length of the cylindrical afterbody. For the

case of the cone-cylinder configuration in axially symmetric inviscid flow, it can be shown that the two-dimensional Prandtl-Meyer expansion just described is indeed valid immediately behind the juncture of cone and cylinder and that thereafter, progressing downstream, the pressure approaches the free-stream value asymptotically. Furthermore, the asymptotic approach to free-stream pressure is very gradual at high Mach numbers. For a cone-cylinder configuration with a 20° conical nose in a flow where $M = 6.86$, the ratio of surface to stream pressure p_{cy}/p_1 can be shown theoretically to change from 0.71 just behind the junction of the cone and cylinder to 0.83 at a point 4 diameters downstream of the junction. Although this change is not negligible, the assumption of a constant surface pressure along a given radial station on the cylindrical portion of a cone-cylinder configuration at a given angle of attack does serve as a useful first approximation.

Changes in pressure due to separation behind the cone-cylinder juncture have very little effect on the over-all characteristics of the model, since in general the low-pressure side contributes but little to the total forces. Also, it is interesting to note the variance between the low pressures on the lee side of a cylinder at hypersonic speeds and the high pressures predicted at lower speeds by theories based on the cross-flow concept.

Hypersonic Approximation

Grimminger, Williams, and Young (reference 6) present a hypersonic approximation to the forces encountered on an inclined body of revolution. This approximation is based on the Newtonian corpuscular theory of aerodynamics and, as its nomenclature implies, is designed for application at very high Mach numbers (greater than 10 or 15). This theory does not predict pressures on that portion of the body shielded from the free air stream; however, by means of an assumption for the pressure in the shielded region, it can be employed at lower Mach numbers for first estimates, although the physical conditions of the problem no longer conform to the initial assumptions. The results of this theory are presented in two forms: the first considers only the simple impact forces encountered by the body, and the second includes the more complex pressure-relieving effect afforded by the centrifugal forces which are introduced by the air flow over the curved surface of the body. In the derivation of the effects of the centrifugal forces on the pressure, five relations are developed for determining the effective velocity distribution over the surface. The fifth relation has been used in the present paper in the theoretical calculations referred to as "Grimminger's hypersonic approximation including centrifugal effects."

Ivey and Morrissette (reference 7) also present an approximate theory for application at very high supersonic speeds which, however,

is applicable only to the cylindrical portions of bodies. It can be shown that Grimminger's hypersonic approximation using case 4 for the centrifugal effects is identical to Ivey's.

RESULTS AND DISCUSSION

Pressure Distributions

As previously indicated, surface pressure distributions were obtained only for the configuration consisting of a 20° conical nose and a cylindrical afterbody having a length-to-diameter ratio of 4.

Axially symmetric case.- In figure 4, the ratio of surface pressure on the body to stream pressure p/p_1 is presented as a function of axial station z/l_t and compared with theoretical calculations. Measurements were made at two angular positions $\beta = 0^\circ$ and $\beta = 90^\circ$ with the configuration in the axially symmetric attitude (that is, $\alpha = 0^\circ$). The results of the Taylor-Maccoll solution were used to determine the theoretical curve for the conical nose, and this solution was extended by the characteristics method including rotational effects to obtain the theoretical curve for the cylindrical afterbody.

In general, the agreement between experimental data and theoretical calculations is good. There is, however, a small difference between the experimental data obtained at the two angular positions, which is attributed to a small error in alining the model with the flow on the two successive runs made to obtain the data. The slight deviation of the pressure of the forepart of the conical nose is considered to be the result of (1) small surface irregularities which were incurred in machining operations and whose effect is accentuated at the tip where the imperfections become relatively large in comparison to the local radius and (2) boundary-layer effects. The discrepancy between theory and experiment that appears in the region of the cone-cylinder junction ($z/l_t = 0.410$) is attributed also to the boundary layer, which, in effect, changes the geometric shape of the body; thus, rather than experiencing the theoretical "instantaneous" expansion at the corner, the flow undergoes a comparatively gradual expansion which originates slightly ahead of the geometric corner and is completed at a point considerably downstream from it. Base-pressure measurements were made, and although no attempt was made during the course of the investigation to obtain experimental verification, it is likely that the sting exerts a significant influence on the base-pressure measurements.

Conical nose at angles of attack.- Experimental and theoretical pressure distributions on the surface of the conical nose are shown in figure 5 in the form of the ratio p_c/p_1 as a function of angular

position β for three angles of attack: 6.7°, 14°, and 20°. For all three angles of attack, the experimental data exhibit a slight variation with axial station which is attributed partly to normal data scatter and partly to boundary-layer influence. In addition, the pressures recorded at station 0.060 are consistently high on the upper portion of the cone and low on the under portion in comparison with pressures measured at the other axial stations. This deviation of the pressure at the foremost axial station is considered to be due to the physical imperfections of the conical tip and to the influence of the boundary layer, both of which effects are magnified near the apex because of the small radius of revolution.

Figure 5(a) shows that at $\alpha = 6.7^\circ$ Ferri's theory is in very good agreement with experiment, although there is a slight overestimation of the pressure on the upper portion of the cone.[1] The theory of Stone-Kopal, while agreeing favorably with experiment at angular positions on the side of the cone, is appreciably low on both the upper and lower surfaces of the cone. Grimminger's hypersonic approximation neglecting centrifugal forces has a tendency to be slightly low in comparison with experiment for all angular positions; the largest divergence, however, occurs on the upper surface. The analysis of the pressure forces encountered on conical and ogival noses, as presented in reference 6, indicates that the pressure-relieving effect of centrifugal forces on such configurations is very small so that the pressures can be satisfactorily approximated by the Newtonian (impact force) method. Consequently, only the results of the latter method, in which centrifugal forces are not included, are presented for the conical nose in the present paper. Nevertheless, it is of interest to note that the inclusion of the centrifugal effect, however small, would augment the discrepancy between theory and experiment.

In figure 5(b), the application of Ferri's theory to the determination of the pressure distribution at $\alpha = 14^\circ$ again compares favorably with experiment except on the upper surface where the theory predicts higher pressures than are obtained experimentally. Because this angle of attack is comparatively large for a first-order theory, the agreement between theory and experiment is an indication that in conical flow at moderate angles of attack, higher-order effects are relatively small at this Mach number. Over the region in which it can be applied, the results from Grimminger's hypersonic approximation neglecting centrifugal forces are in good agreement with experimental results.

---

[1]It may be noted that there is a difference between the theoretical curves presented in this paper and those presented in Ferri's work (reference 3) for the same Mach number and model configuration. This is due to the high sensitivity of the calculations to small variations in the initial values obtained from Kopal's table (reference 5) and in the entropy determination.

In figure 5(c), Ferri's theory has been presented so that some estimate of the higher-order effects at this high angle of attack ($\alpha = 20^\circ$) could be made. While these effects are by no means negligible here, it is seen that the first-order theory may still be employed to determine an approximation to the pressure distribution. As in the case of $\alpha = 14^\circ$, Grimminger's hypersonic approximation neglecting centrifugal effects is in good agreement with experiment over the radial positions for which it is applicable.

Cylindrical afterbody at angles of attack.- Pressure distributions on the cylindrical afterbody of the configuration with the 20° conical nose at three angles of attack are presented and compared with theory in figure 6. The boundary-layer effect, which prevents the expansion from occurring instantaneously at the cone-cylinder junction, appears at all angles of attack with the result that pressures measured at station 0.430 are significantly higher than those obtained at the other stations.

Figure 6(a) shows that at $\alpha = 6.7^\circ$ the extension of Ferri's cone theory by considering the flow to undergo a two-dimensional expansion from the conical surface to the cylindrical surface gives very good agreement with theory except over the upper portion of the cylinder, since the theoretical calculations considerably underestimate experimental values on the upper portion of the cone. Grimminger's hypersonic approximation neglecting centrifugal effects is in fair agreement with experiment except at the side and bottom positions. Inclusion of the centrifugal effects improves the agreement over most of the lower portion of the cylinder but does not alter the discrepancy at the side or bottom. The centrifugal forces as treated in Ivey's hypersonic approximation clearly overestimate the pressure-relieving effect at this angle of attack and Mach number. The result is a theoretical pressure prediction which decreases too rapidly from a pressure equal to that obtained by Grimminger's approximation at the bottom position ($\beta = 180^\circ$) to a pressure that is much too low along the sides of the cylinder.

At $\alpha = 14^\circ$, as shown in figure 6(b), the extension of Ferri's cone theory, although slightly low, still gives a favorable agreement with experiment. Grimminger's hypersonic approximation neglecting centrifugal forces is considerably higher than experiment, particularly at the bottom of the cylinder ($\beta = 180^\circ$). Including the effect of the centrifugal forces somewhat improves the agreement between theory and experiment; however, as the centrifugal forces have no effect on the pressure at $\beta = 180^\circ$, the rather poor agreement there remains unaltered. Again, it is observed that Ivey's hypersonic approximation overestimates the effect of the centrifugal forces.

Figure 6(c) shows essentially the same comparison between theory and experiment at $\alpha = 20^\circ$ as was obtained at $\alpha = 14^\circ$. Since at high

angles of attack, as expected, Ferri's cone theory gives poor results, the extension of this theory to the cylindrical surface at $\alpha = 20^\circ$ gives extremely poor agreement and is therefore not presented in the figure.

Model base.- In figure 7, experimental pressures measured on the base of the cone-cylinder configuration at four angles of attack are shown. At both $\alpha = 6.7^\circ$ and $\alpha = 14^\circ$ the base-pressure distribution is essentially constant at approximately 0.23, while at $\alpha = 20^\circ$ there appears to be a low-amplitude sinusoidal variation about an average pressure ratio of 0.7. The pressures obtained at two angular positions $\beta = 0^\circ$ and $\beta = 90^\circ$ for $\alpha = 0^\circ$ indicate that in this case also there is a small variation of the radial pressure distribution.

Figure 8 shows the variation of the averaged base-pressure data with angle of attack. This variation of base pressure on a sting-supported cone-cylinder configuration in wind-tunnel tests constitutes a rather complex problem which, although of great interest both theoretically and practically, was considered to be beyond the scope of the present investigation.

Aerodynamic Forces

Local normal force.- The axial variation of the local normal-force coefficient c_n for the 20° cone-cylinder configuration is presented in figure 9 as obtained from pressure measurements and referred to the base area. The linear variation of c_n on the conical nose is maintained for all three angles of attack; the small variation from linearity observed at station 0.06 is a result of the imperfect tip and of boundary-layer effects, as previously mentioned in the discussion of pressure distributions. On the cylindrical afterbody, an almost constant c_n is obtained except at station 0.434, where boundary-layer effects most severely alter the pressure distribution. It should be emphasized that this constancy of c_n along the cylindrical portion is a characteristic only of very high speed flows and is not obtained at low supersonic Mach numbers.

At $\alpha = 6.7^\circ$, the integration of the conical-nose pressure distribution obtained by Ferri's theory yields local normal coefficients slightly lower than the experimental results. Comparison with figure 5(a) shows that this theory overestimates the pressures on the upper surface of the cone and the reduction in normal force is a direct consequence of this discrepancy in pressure distribution. The pressure distributions predicted by Ferri's theory at $\alpha = 14^\circ$ and $\alpha = 20^\circ$ account for the progressively poorer absolute agreement of the theoretical and experimental c_n. The discrepancies in pressure distribution obtained at $\alpha = 6.7^\circ$ by the Stone-Kopal theory prove to be

compensatory so that integrated results are in excellent agreement with experimental results. Since this first-order theory predicts a linear variation with angle of attack of the normal force encountered by a cone, the excellent results obtained at the low angle of attack where the theory is applicable can be extended to the higher angles with good results which verify the first-order linearity. As shown in figure 9, Grimminger's hypersonic approximation neglecting centrifugal force effects also shows excellent agreement with experiment when applied to the conical nose.

At $\alpha = 6.7^{\circ}$, the results of Ferri's theory and Grimminger's hypersonic approximation neglecting centrifugal forces extended to the cylinder are in good agreement with each other and only slightly higher than the experimental results. The inclusion of the effects of centrifugal forces, which decreases the normal force by 10 percent, brings theory and experiment into almost perfect agreement; however, at $\alpha = 14^{\circ}$, Ferri's cone theory extended agrees well with experiment whereas Grimminger's hypersonic approximation, even with centrifugal effects included, overestimates the normal forces. Comparison with the pressure distributions in figures 6(b) and 6(c) discloses that the major portion of this discrepancy between the Grimminger theory and experiment is a result of the theory's overestimating the pressures on the bottom of the cylinder.

Lift, drag, and lift-drag ratios.- In the theoretical calculation of the aerodynamic force coefficients, a base pressure of one-half the stream pressure was used in all cases. (Consideration of the base-pressure distributions shown in figures 7 and 8 led to the selection of this value for use in theoretical calculations.) The effect of the forces contributed by the base pressures on the over-all aerodynamic characteristics of the configurations is negligibly small except in the case of the drag coefficient at very low angles of attack, where the force on the base is about 5 percent of the total C_D. Therefore, a more detailed investigation of base pressures was not considered necessary for the purposes of the present paper.

The aerodynamic coefficients based on Grimminger's hypersonic approximation including centrifugal forces have not been included in figures 10 to 13. The centrifugal forces decrease the normal forces encountered on the cylindrical afterbody by 10 percent, thereby decreasing the total normal force by about 5 percent for the longest cone-cylinder configuration at angles of attack greater than about 15°. This results in a decrease in both C_L and C_D; however, for angles of attack below 10°, this decrease in over-all coefficients is negligible.

The variation with angle of attack of the aerodynamic characteristics of the 20° cone, determined experimentally by both pressure and force tests, is presented in figure 10. (Pressure distributions on the

conical nose as obtained in the test of the cone-cylinder configuration with $\frac{l}{d} = 4$ were used in determining the aerodynamic characteristics of the cone alone.) Through the angle-of-attack range for which it is applicable, that is, up to about $\alpha = 10^{\circ}$, Ferri's theory is in good agreement with the experimental drag coefficient C_D although it is somewhat low with respect to the experimental lift coefficient C_L and, consequently, with respect to the lift-drag ratio L/D. On the other hand, Grimminger's theory neglecting centrifugal forces is in excellent agreement with experimental C_D at high angles of attack and slightly low at the smaller angles; however, it overestimates C_L throughout the entire range, resulting in lift-drag ratios which are high. The C_D value obtained from the Stone-Kopal theory is slightly low at angles of attack beyond 4° and, although not shown here, the Stone-Kopal C_L is almost coincident with the Grimminger values for angles of attack up to 10°.

Figure 11 presents the variation with angle of attack of the aerodynamic characteristics of the 20° cone-cylinder for which $\frac{l}{d} = 2$. Again, Ferri's theory plus its extension to the cylindrical surface is in excellent agreement with experiment up to about $\alpha = 10^{\circ}$. Grimminger's hypersonic approximation agrees satisfactorily with experimental C_D at the higher angles of attack though it is slightly low at the lower angles. As in the case of the cone alone, the Grimminger approximation overestimates C_L at the higher angles.

Figure 12 shows the variation with angle of attack of the aerodynamic characteristics of the 20° cone-cylinder for which $\frac{l}{d} = 4$. For this configuration, both theories compare with experiment in much the same manner as for the $\frac{l}{d} = 2$ configuration except that, in this case, Ferri's theory plus its extension to the cylindrical surface slightly overestimates C_L at the low angles of attack, resulting in lift-drag ratios which are too large in this range.

Comparison of the three configurations.- In figure 13, the experimentally determined aerodynamic characteristics of the three configurations have been presented in a manner that facilitates their mutual comparison. Figure 13(a) shows that the C_L curve for the cone without afterbody is essentially linear with angle of attack but has a slight bend downward; the addition of the cylindrical afterbody significantly increases the lift and, in addition, produces lift curves with a slightly upward curvature. This curvature appears most distinctly at high angles of attack and increases with increasing cylindrical-afterbody length. The drag coefficients and lift-drag ratios are shown in figure 13(b).

The increment between the results for the cone and the cone-cylinder configurations represents the drag due to the addition of the cylindrical afterbodies. The agreement between the force and pressure data for a given configuration discloses no significant discrepancies, indicating that the viscous forces are very small in comparison with the pressure forces on all three configurations. This is further emphasized by the fact that the minimum drags (at $\alpha = 0^{\circ}$) for the three configurations were not measurably different. The plot of the lift-drag ratios shows that a significant increase in L/D can be obtained by adding a cylindrical afterbody to a cone. The L/D curves for all three configurations have nearly flat maximums, and while $(L/D)_{max}$ varies from about 1.8 for the cone alone to 2.4 for the cone-cylinder configuration with $\frac{l}{d} = 4$, the angle of attack at which $(L/D)_{max}$ occurs remains essentially constant at about $\alpha = 10^{\circ}$. The limiting L/D curve shown in figure 13(b) is equivalent to the lift-drag ratio that is obtained as l/d approaches infinity for any cone-cylinder configuration if viscous forces are not included.

In figure 13(c), the pitching-moment coefficients and the location of the centers of pressure of the three configurations as determined experimentally are presented as a function of angle of attack. As the cylindrical-afterbody length is increased, the center of pressure moves forward. For a given cone-cylinder configuration, the center of pressure moves slightly rearward with increasing angle of attack.

A comparison of theoretical with experimental results for pitching moment and center of pressure can best be obtained by again utilizing figure 9, since merely adding theoretical curves to figure 13(c) would only tend to obscure the results. In the case of the cone, the center of pressure for all the theories, as would be expected, agrees with that determined experimentally; however, the pitching-moment coefficients are not predicted as well because in the case of the cone alone these depend on the accuracy of the prediction of the normal-force coefficient. An examination of figure 9 shows that this coefficient for the conical nose is given best by the Stone-Kopal theory and the Grimminger hypersonic approximation and with less accuracy by Ferri's theory. When the afterbodies are included, a comparison with the results produced by a Prandtl-Meyer expansion at the cone-cylinder juncture and an invariant axial pressure has been resorted to as shown by figure 9. With an afterbody length of 4 diameters, which is the worst case of the test bodies for this assumption, none of the theories predicts centers of pressure which are more than about 2 percent of the body length from the experimental results (using Ferri's theory up to 14° only). In the prediction of moment coefficient, Ferri's theory and Grimminger's hypersonic approximation with centrifugal forces give better results than Grimminger's hypersonic approximation without centrifugal forces;

however, even the theories in best agreement are 10 percent in error at $\alpha = 14^{\circ}$.

The effect on the minimum drag of varying the apex angle.- Figure 14 shows the results of the tests of the second series of configurations which consisted of conical noses with apex angles varying from 10° to 180° and with identical cylindrical afterbodies of 4 diameters length. These configurations were tested only in the zero lift ($\alpha = 0^{\circ}$) attitude. The theoretical drag curve presented in this figure was determined by using the Taylor-Maccoll solution on the surface of the cone and assuming the base pressure equal to the free-stream pressure. Because of the small forces encountered on the $\theta = 10^{\circ}$ and $\theta = 20^{\circ}$ configurations, it was possible to use a more sensitive force balance and thereby obtain more accurate force measurements for these two bodies in comparison with the balance used and measurements made on the remaining bodies. When a base-pressure ratio of 0.75 (the value actually measured for the configuration with $\theta = 20^{\circ}$) is included and when viscous effects estimated from laminar-boundary-layer considerations are introduced, theoretical calculations and experimental measurements for the two low-angle bodies are brought into nearly exact agreement. At the higher cone angles, satisfactory agreement was obtained with the results from Taylor-Maccoll cone theory which at this Mach number is applicable up to about $\theta = 100^{\circ}$. The results of the blunt-body test ($\theta = 180^{\circ}$) indicate that the average pressure on the face of the body was slightly higher than the static pressure behind a normal shock at $M = 6.86$. The actual pressure distribution on the face must decrease from the stagnation pressure behind a normal shock at the center to some value considerably lower at the periphery. Furthermore, some curvature of the shock was present just ahead of the periphery, resulting in a reduced pressure drag.

Schlieren Photographs

In figure 15, schlieren photographs of the 20° cone and cone-cylinder configurations at several angles of attack are shown. The lower surface of the conical shock appears strong and clearly defined, as expected. The upper surface of the shock is rather indistinct in most of the photographs since its strength is approaching that of a Mach wave. For those configurations with afterbodies at high angles of attack, the lower surface of the shock becomes nearly parallel to the body axis.

Schlieren photographs of cone-cylinder configurations with progressively increasing cone angles and cylindrical afterbodies with $\frac{l}{d} = 4$ are shown for $\alpha = 0$ in figure 16. This series of pictures illustrates the influence of the expansion which occurs at the cone-cylinder

junction on the shock which originates at the cone apex. The point at which influence is felt can be identified as the position at which the uninfluenced straight conical shock begins to curve. This point moves from a position beyond the field of view in the case of $\theta = 10^{\circ}$ to a position just downstream from the junction in the case of $\theta = 90^{\circ}$. For $\theta = 180^{\circ}$, the shock detaches and assumes the shape of a very flat paraboloid. Since the nose of this detached paraboloidal shock is normal to the free stream, subsonic flow must exist behind it.

CONCLUSIONS

Analysis of experimental data obtained from the wind-tunnel tests of cone-cylinder configurations at $M = 6.86$ and a Reynolds number of 290,000 based on the maximum diameter leads to the following conclusions:

1. Pressure distributions on cone-cylinder configurations in axially symmetric flow can be predicted with a high degree of accuracy by employing the Taylor-Maccoll cone solution and extending it over the cylinder by the method of characteristics for three-dimensional rotational flow; however, at the cone-cylinder junction, boundary-layer effects alter the nature of the expansion so that instead of occurring "instantaneously" as theoretically calculated, the flow undergoes a gradual expansion over a finite distance.

2. Ferri's theory for flow about inclined cones (NACA TN 2236) can be used to determine pressure distributions with very good results at small angles of attack. Even when the angle of attack can no longer be considered small within the first-order approximation, the results are still quite satisfactory, indicating that second-order effects remain small at moderate angles of attack (up to about $\alpha = 15^{\circ}$).

3. Although results of the Stone-Kopal first-order theory are known to be in error, the discrepancies are compensatory with respect to the normal force, and the initial slope of the lift curve is satisfactorily predicted.

4. The hypersonic approximation of Grimminger, Williams, and Young neglecting centrifugal forces satisfactorily predicts pressure distributions on cones throughout the angle-of-attack range over the windward side.

5. When the pressure distribution on the conical nose at a given angle of attack is known, a good approximation to the pressure distribution on the cylindrical afterbody can be made by considering a simple Prandtl-Meyer expansion of the flow around the corner formed by the

cone-cylinder junction, since at very high Mach numbers the pressures on the cylindrical afterbody vary slowly with respect to axial station.

6. The hypersonic approximation of Grimminger, Williams, and Young with modifications can be used to predict pressure distributions on the windward side of the cylindrical afterbody; however, there is a decided tendency to overestimate the pressure on the lower surface.

7. The addition of the cylindrical afterbody to the conical nose results in a considerable increase in the lift-drag ratio of the configuration.

8. The theory of Grimminger, Williams, and Young satisfactorily predicts the drag coefficients for all configurations tested throughout the angle-of-attack range; however, it slightly overestimates the lift coefficients and, consequently, the lift-drag ratios.

Langley Aeronautical Laboratory
National Advisory Committee for Aeronautics
Langley Field, Va.

REFERENCES

1. McLellan, Charles H., Williams, Thomas W., and Beckwith, Ivan E.: Investigation of the Flow through a Single-Stage Two-Dimensional Nozzle in the Langley 11-Inch Hypersonic Tunnel. NACA TN 2223, 1950.

2. McLellan, Charles H., Bertram, Mitchel H., and Moore, John A.: An Investigation of Four Wings of Square Plan Form at a Mach Number of 6.86 in the Langley 11-Inch Hypersonic Tunnel. NACA RM L51D17, 1951.

3. Ferri, Antonio: Supersonic Flow around Circular Cones at Angles of Attack. NACA TN 2236, 1950.

4. Stone, A. H.: On Supersonic Flow past a Slightly Yawing Cone. Jour. Math. and Phys., vol. XXVII, no. 1, April 1948, pp. 67-81.

5. Staff of the Computing Section, Center of Analysis (Under Direction of Zdeněk Kopal): Tables of Supersonic Flow around Yawing Cones. Tech. Rep. No. 3, M.I.T., 1947.

6. Grimminger, G., Williams, E. P., and Young, G. B. W.: Lift on Inclined Bodies of Revolution in Hypersonic Flow. Jour. Aero. Sci., vol. 17, no. 11, Nov. 1950, pp. 675-690.

7. Ivey, H. Reese, and Morrissette, Robert R.: An Approximate Determination of the Lift of Slender Cylindrical Bodies and Wing-Body Combinations at Very High Supersonic Speeds. NACA TN 1740, 1948.

8. Taylor, G. I., and Maccoll, J. W.: The Air Pressure on a Cone Moving at High Speeds. Proc. Roy. Soc. (London), ser. A, vol. 139, no. 838, Feb. 1, 1933, pp. 278-311.

9. McLellan, Charles H., Williams, Thomas W., and Bertram, Mitchel H.: Investigation of a Two-Step Nozzle in the Langley 11-Inch Hypersonic Tunnel. NACA TN 2171, 1950.

10. Staff of the Computing Section, Center of Analysis (Under Direction of Zdeněk Kopal): Tables of Supersonic Flow around Cones. Tech. Rep. No. 1, M.I.T., 1947.

11. Isenberg, J. S.: The Method of Characteristics in Compressible Flow. Part I (Steady Supersonic Flow). Tech. Rep. No. F-TR-1173A-ND, ATI No. 26341, Air Materiel Command, U. S. Air Force, Dec. 1947.

12. Staff of the Computing Section, Center of Analysis (Under Direction of Zdeněk Kopal): Tables of Supersonic Flow around Cones of Large Yaw. Tech. Rep. No. 5, M.I.T., 1949.

13. Tsien, Hsue-Shen: Supersonic Flow over an Inclined Body of Revolution. Jour. Aero. Sci., vol. 5, no. 12, Oct. 1938, pp. 480-483.

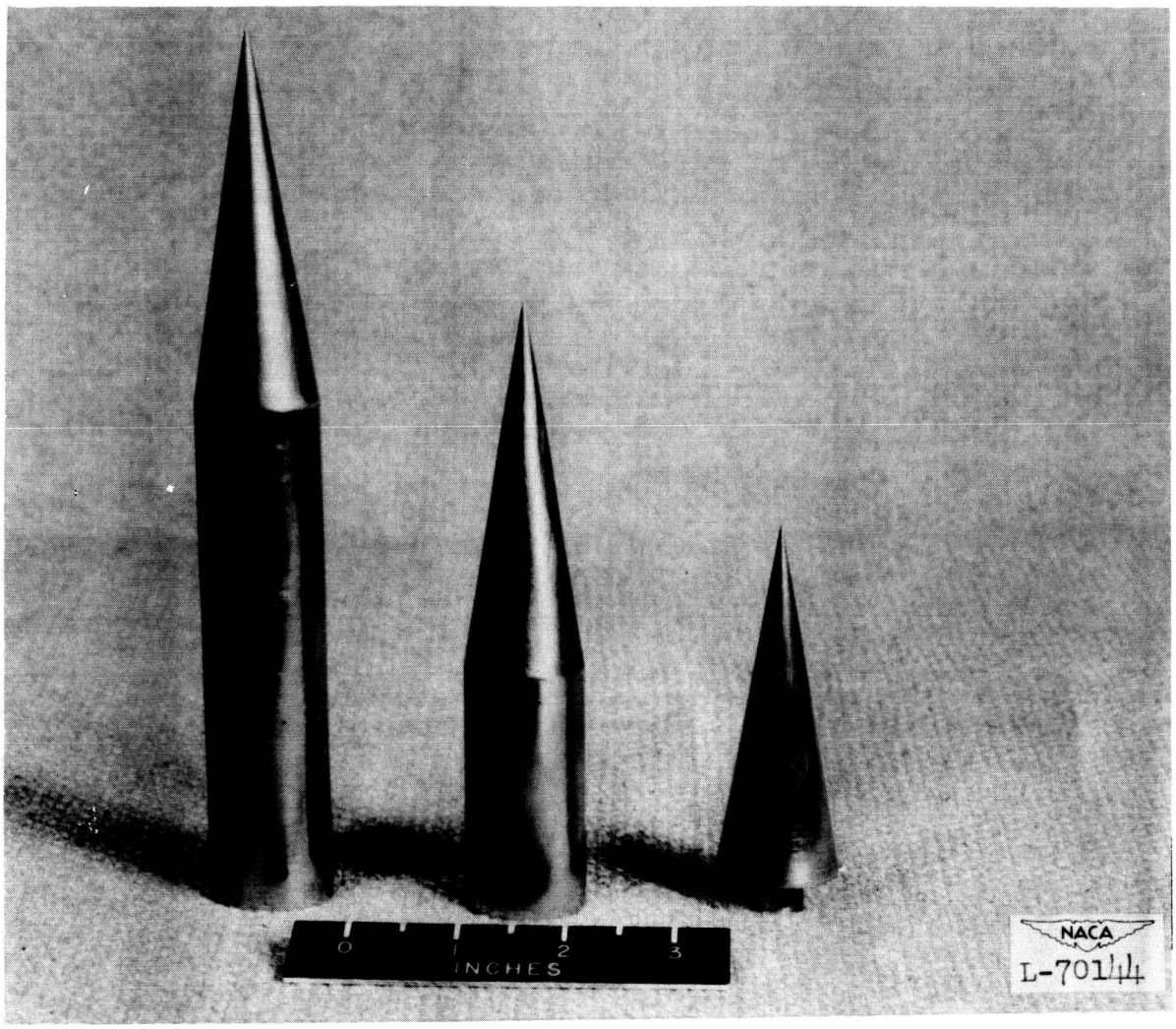

Figure 1.- Force models with apex angle of 20° and afterbody lengths of 4, 2, and 0 diameters.

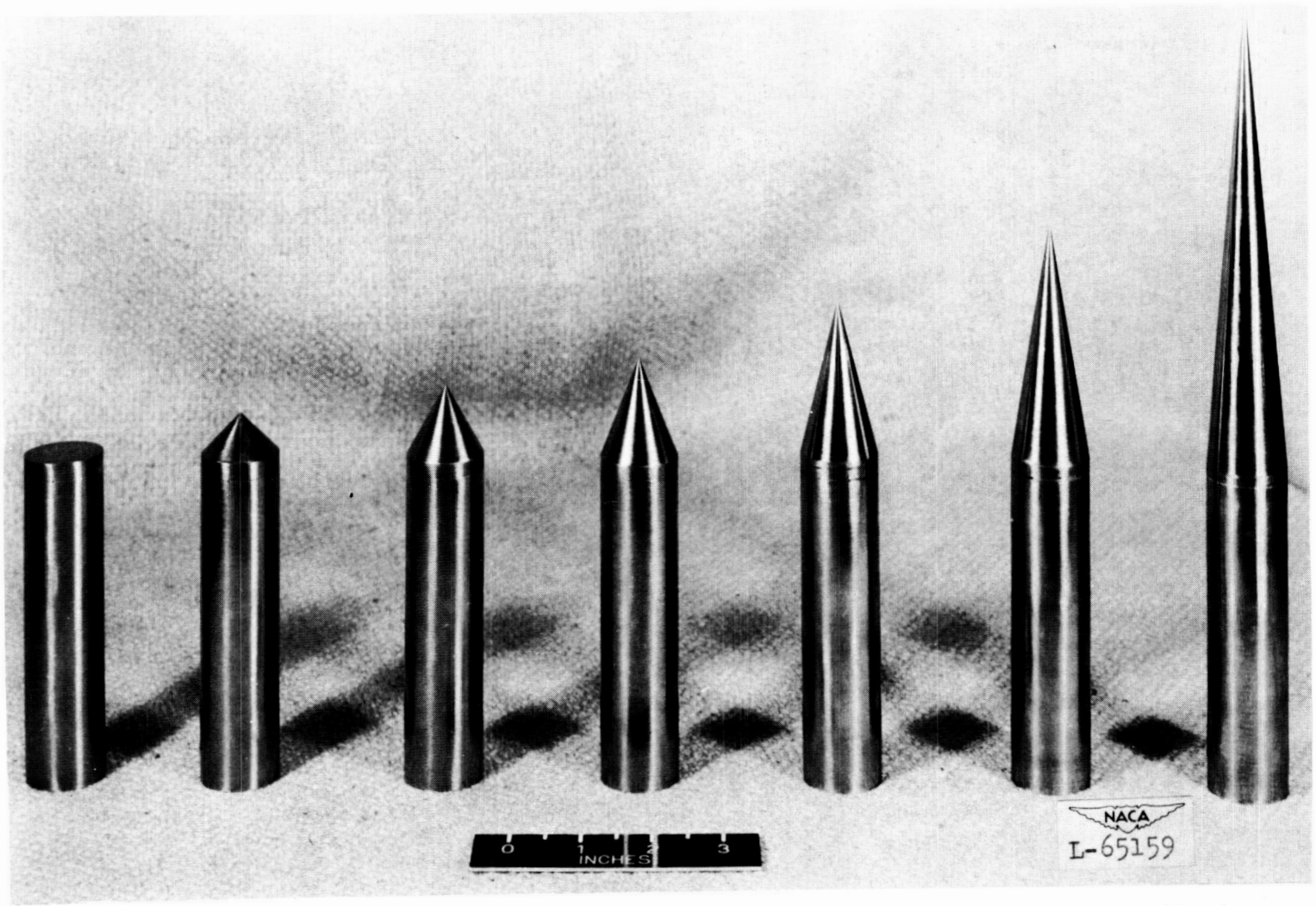

Figure 2.- Force models with varying apex angles and cylindrical afterbodies with a length equal to 4 diameters.

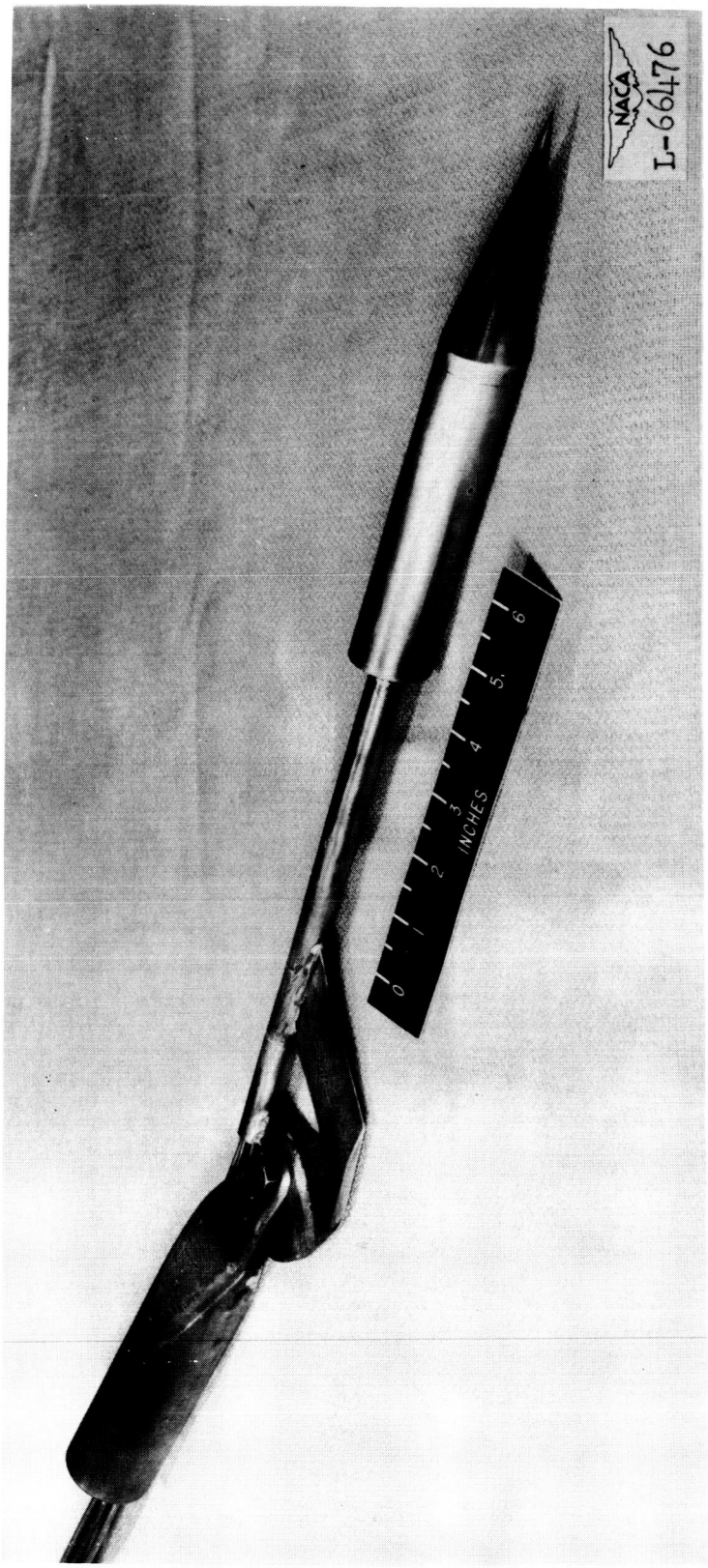

Figure 3.- Pressure model mounted on support sting. Conical nose has 20° apex angle; length of cylindrical afterbody is equal to 4 diameters.

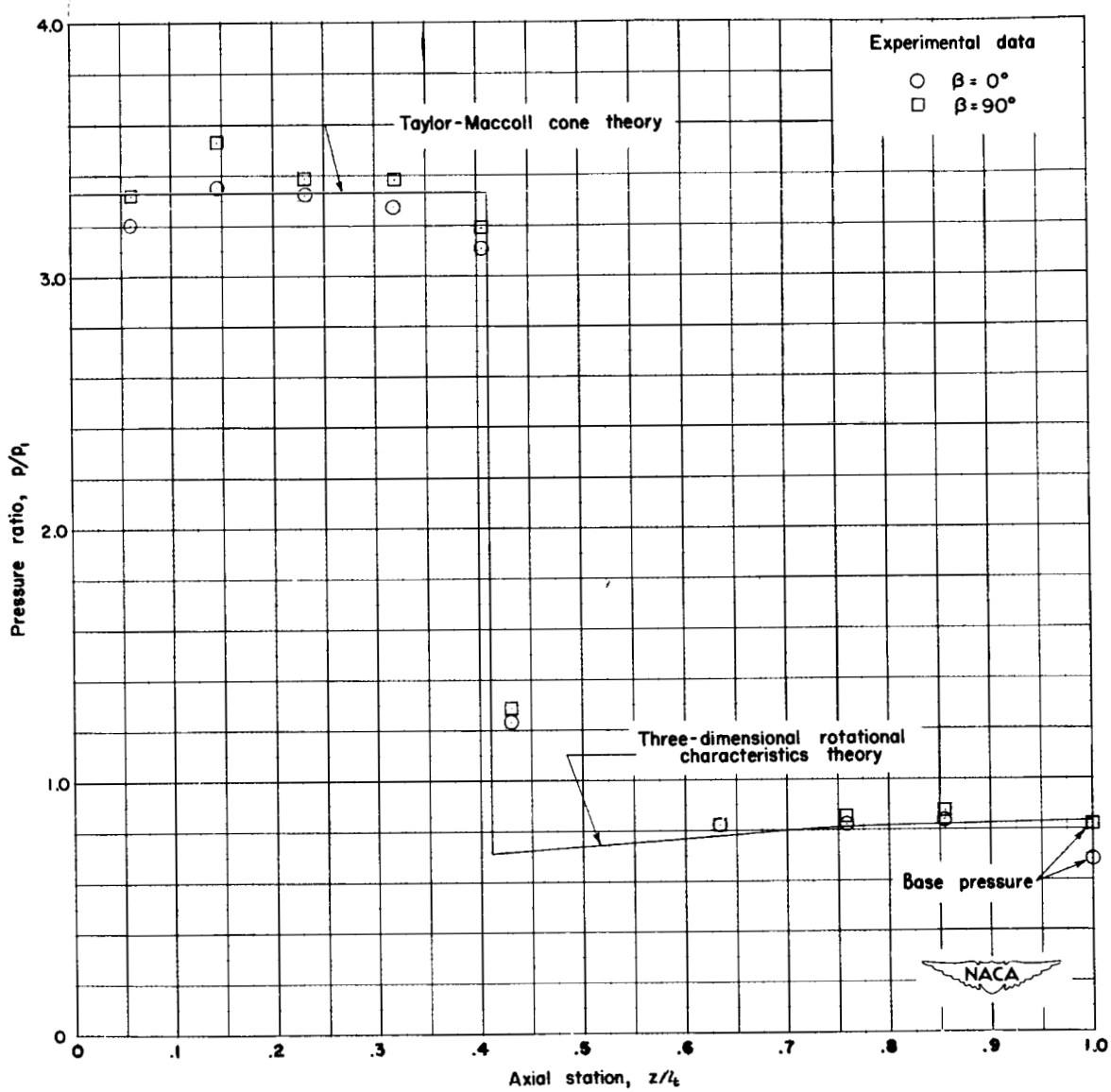

Figure 4.- Axial variation of the ratio of surface to stream pressure for the 20° cone cylinder with $\frac{l}{d} = 4$ at zero angle of attack. M = 6.86.

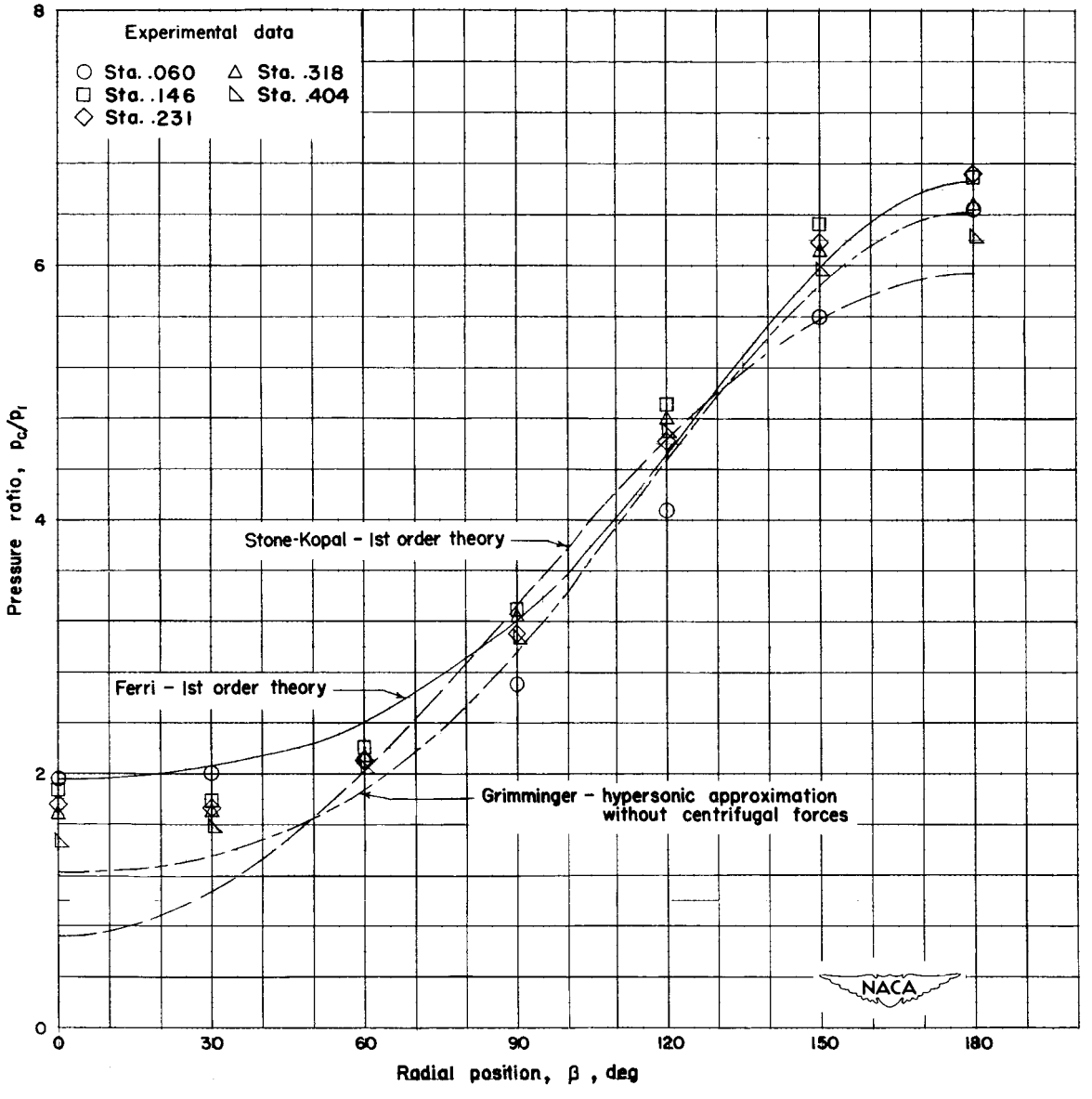

(a) $\alpha = 6.7^{\circ}$.

Figure 5.- Radial variation of the ratio of surface to stream pressure for the conical nose of the 20° cone cylinder with $\frac{l}{d} = 4$. M = 6.86.

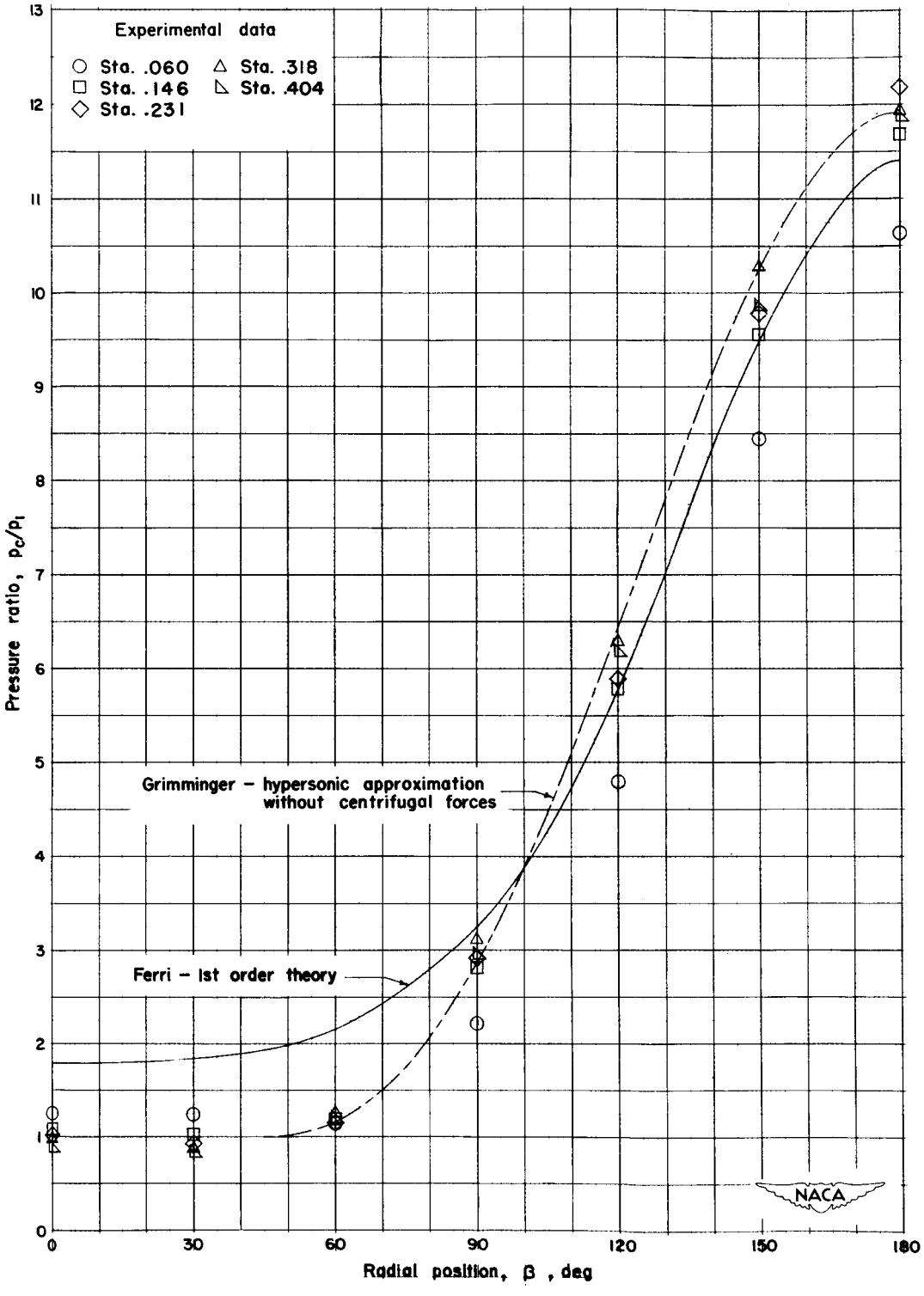

(b) $\alpha = 14^{\circ}$.

Figure 5.- Continued.

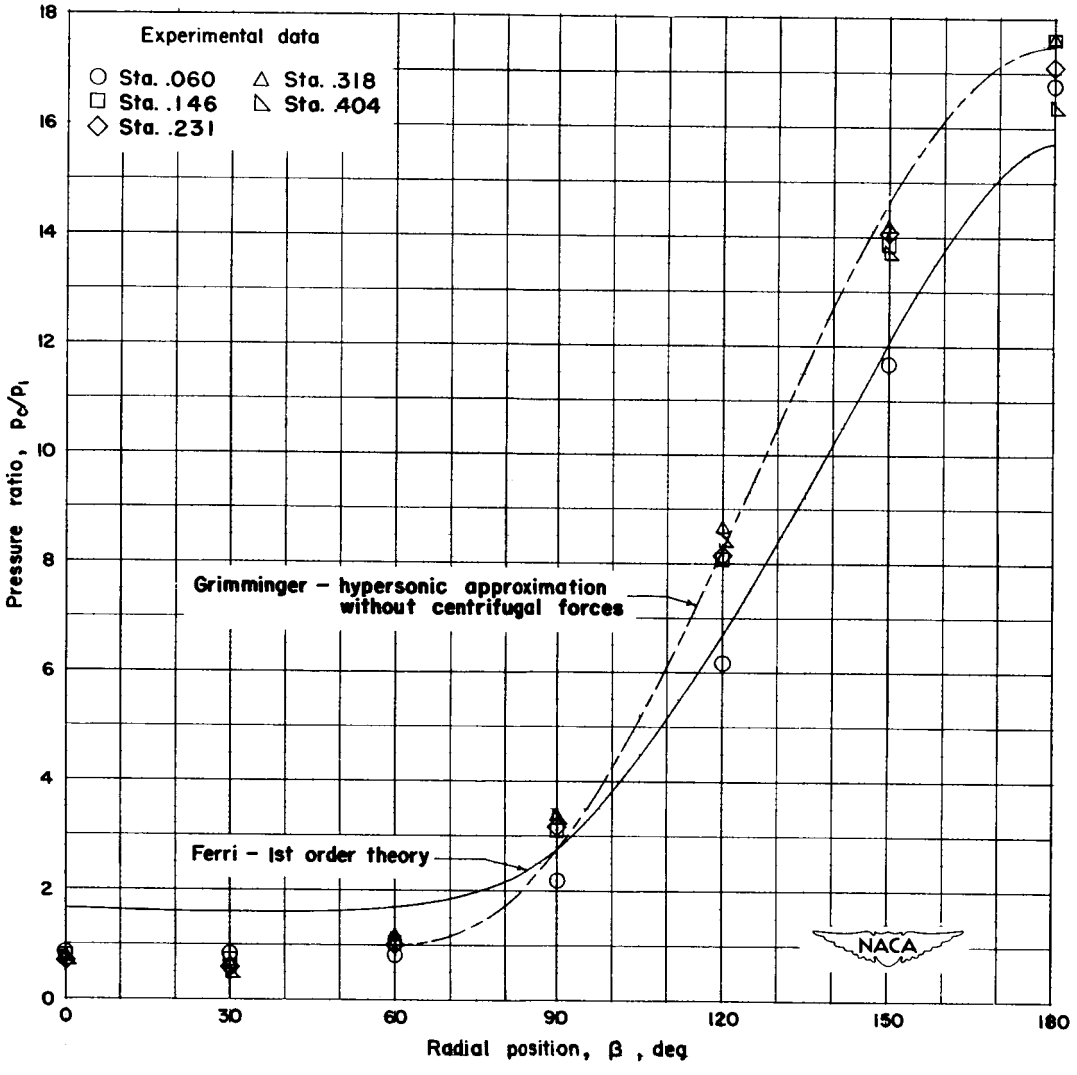

(c) $\alpha = 20^{\circ}$.

Figure 5.- Concluded.

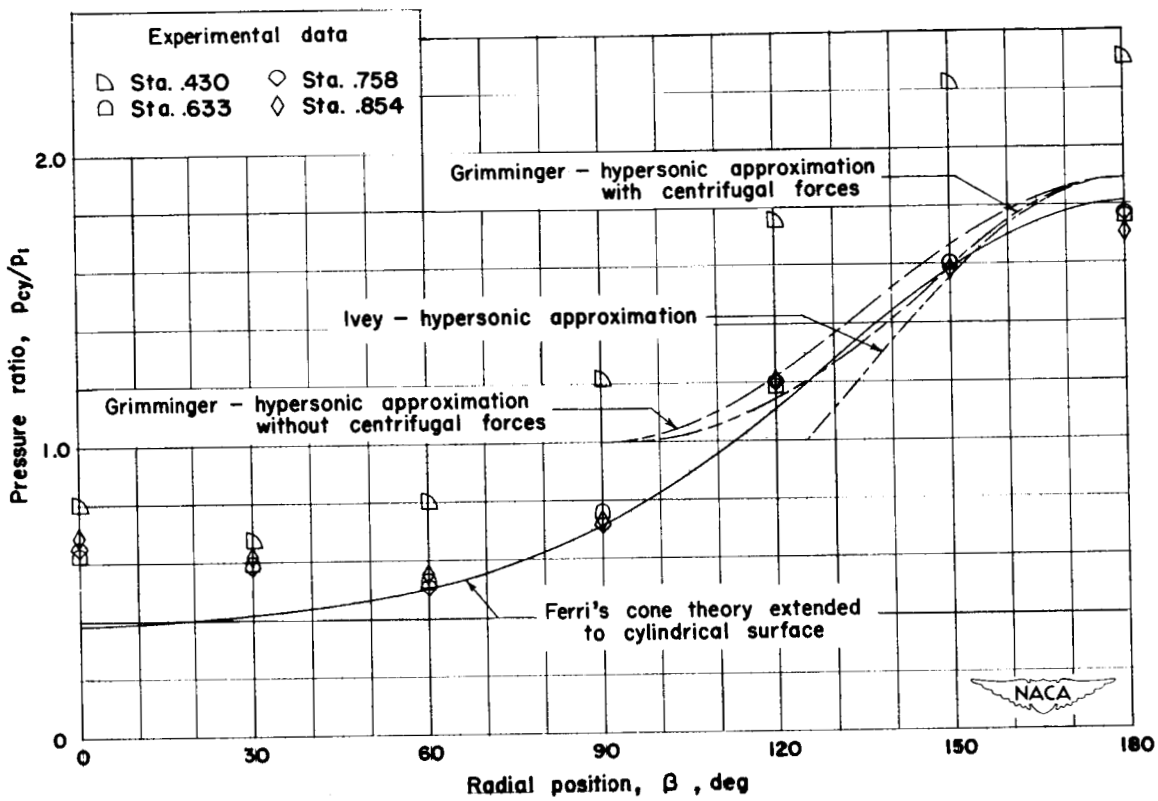

(a) $\alpha = 6.7^{\circ}$.

Figure 6.- Radial variation of the ratio of surface to stream pressure for the cylindrical afterbody of the 20° cone cylinder with $\frac{l}{d} = 4$. M = 6.86.

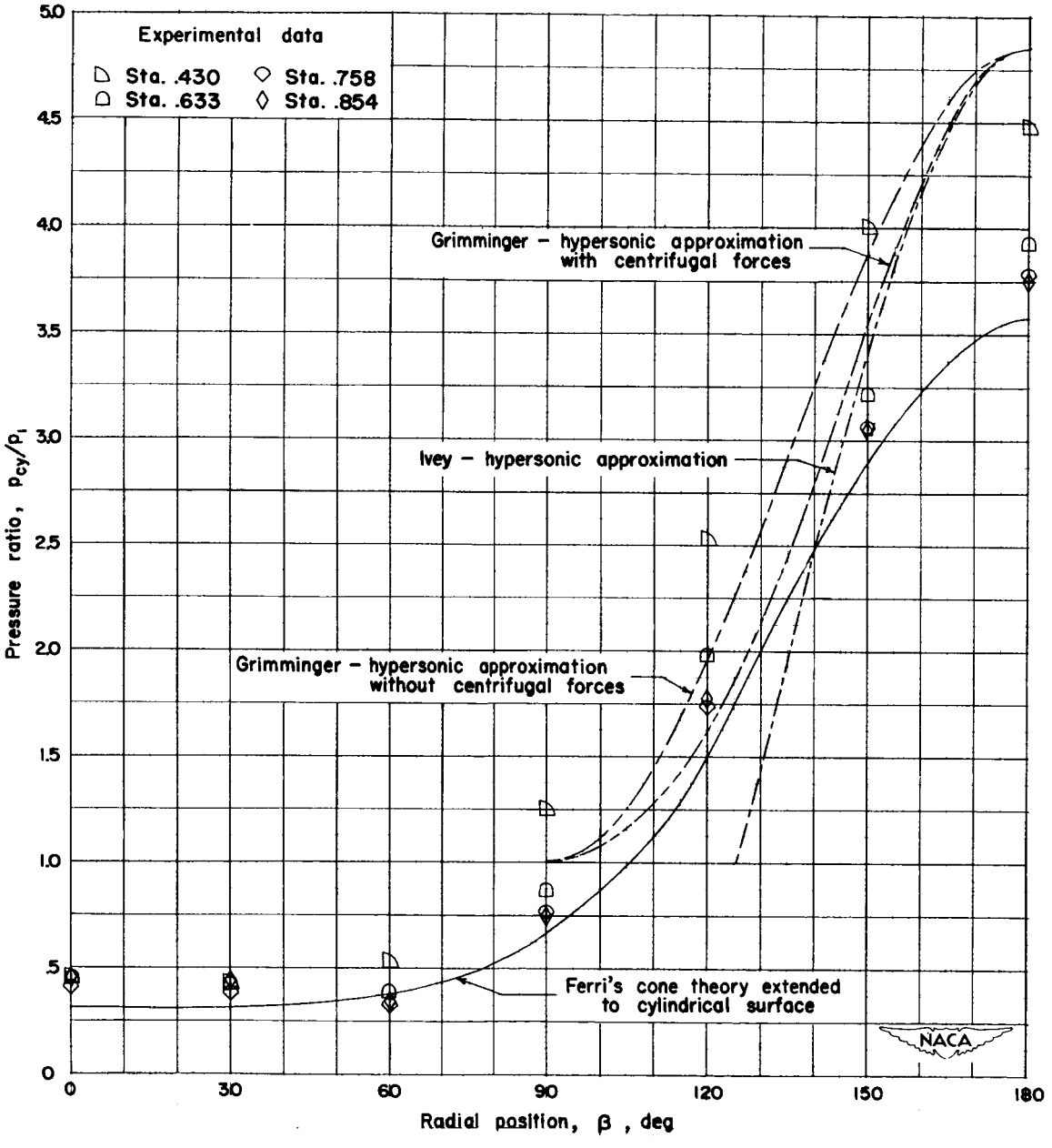

(b) $\alpha = 14^{\circ}$.

Figure 6.- Continued.

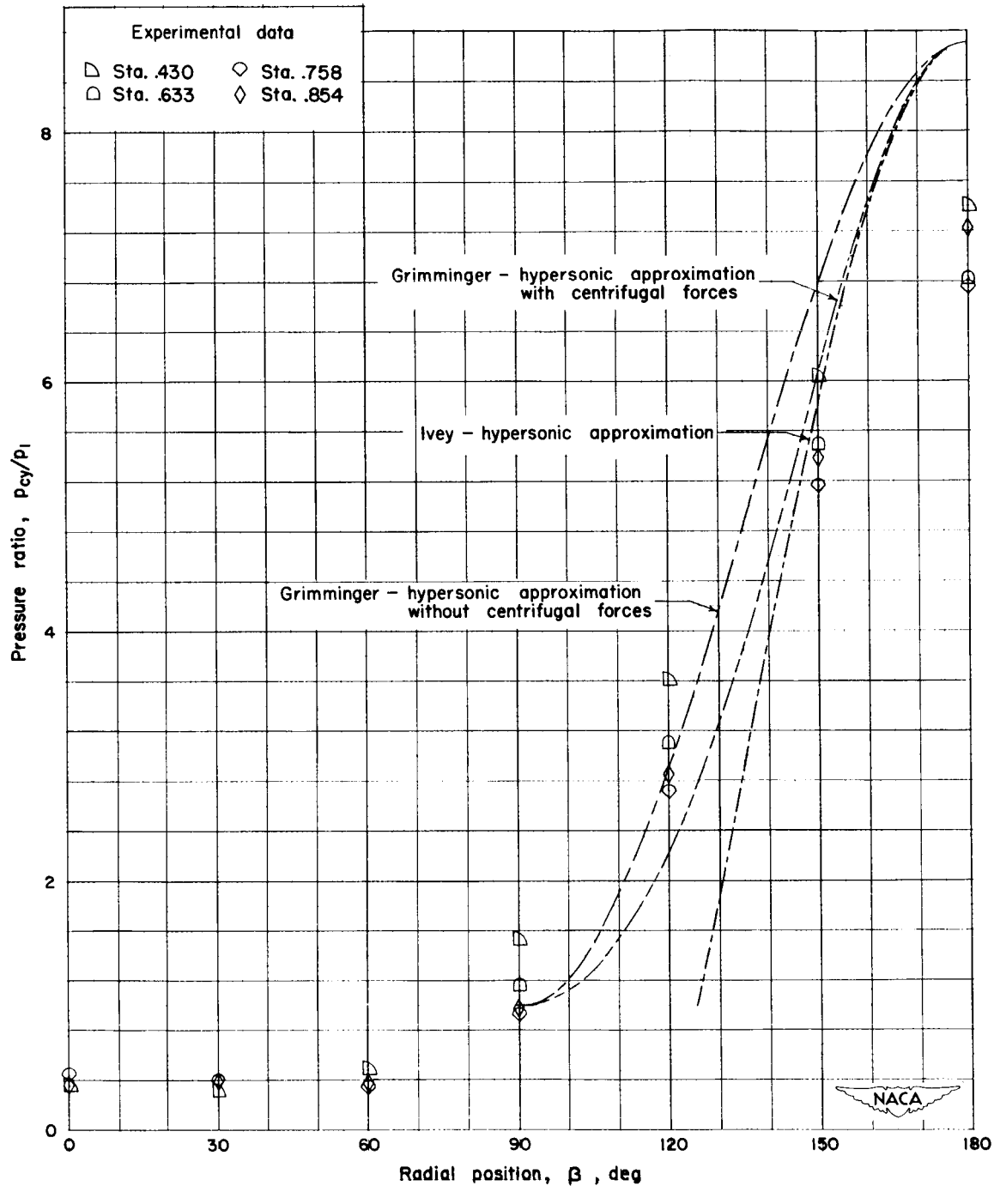

(c) $\alpha = 20^\circ$.

Figure 6.- Concluded.

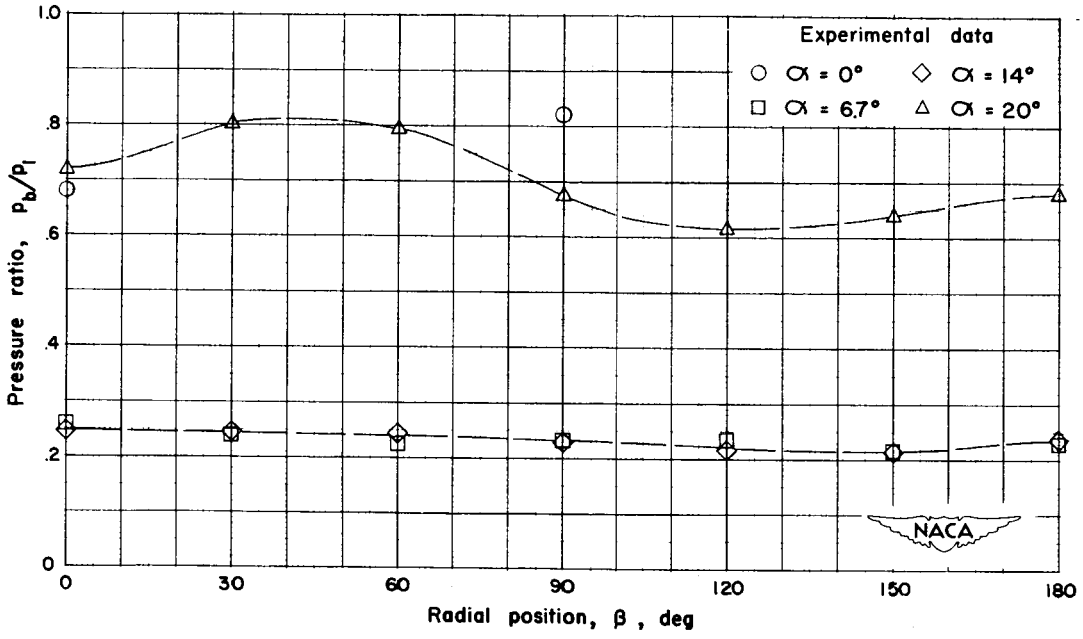

Figure 7.- Radial variation of the ratio of base to stream pressure for the 20° cone cylinder with $\frac{l}{d} = 4$. M = 6.86.

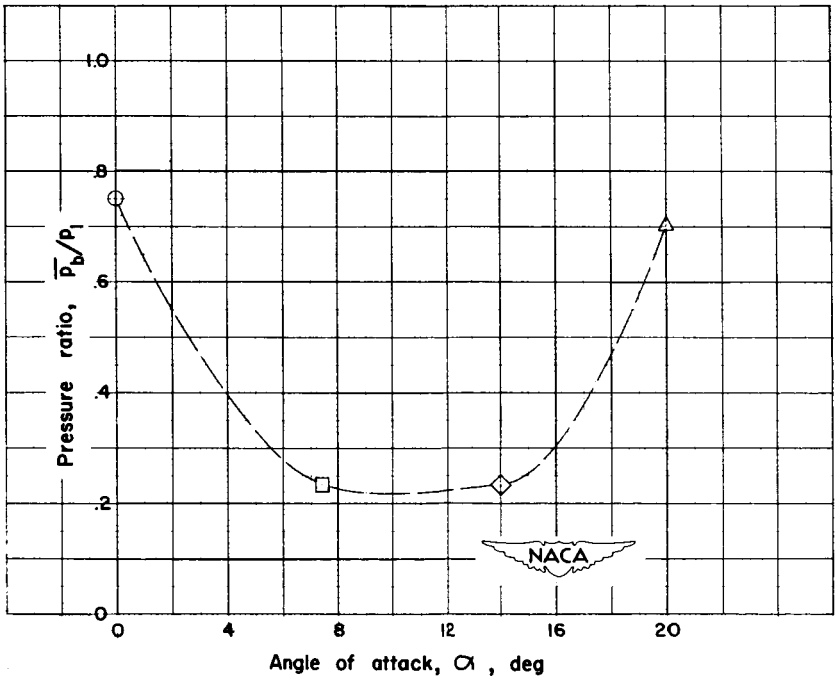

Figure 8.- Variation with angle of attack of the ratio of average radial base pressure to stream pressure for the 20° cone cylinder with $\frac{l}{d} = 4$. M = 6.86.

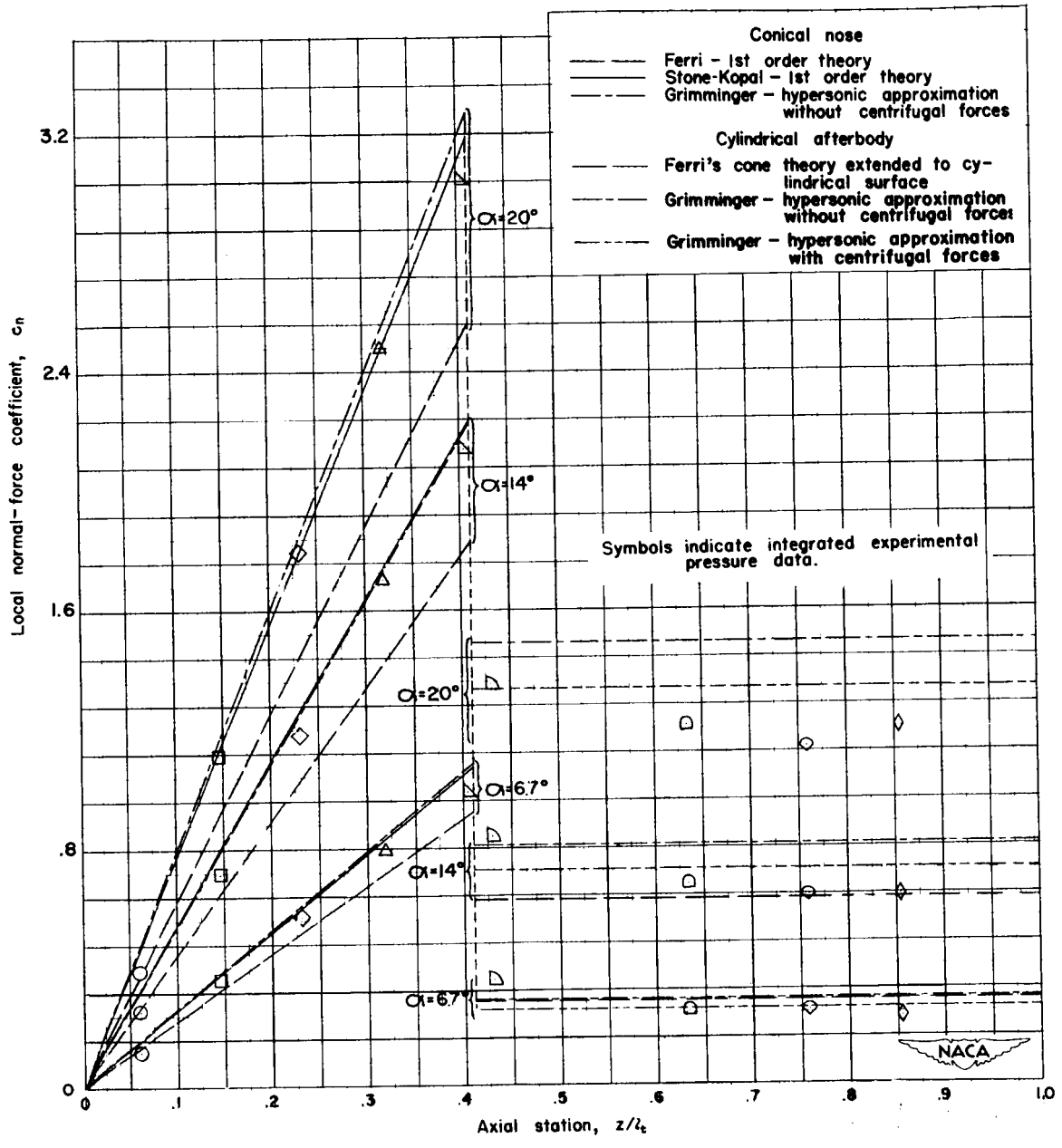

Figure 9.- Axial variation of the local normal-force coefficient of the 20° cone cylinder with $\frac{l}{d} = 4$. M = 6.86.

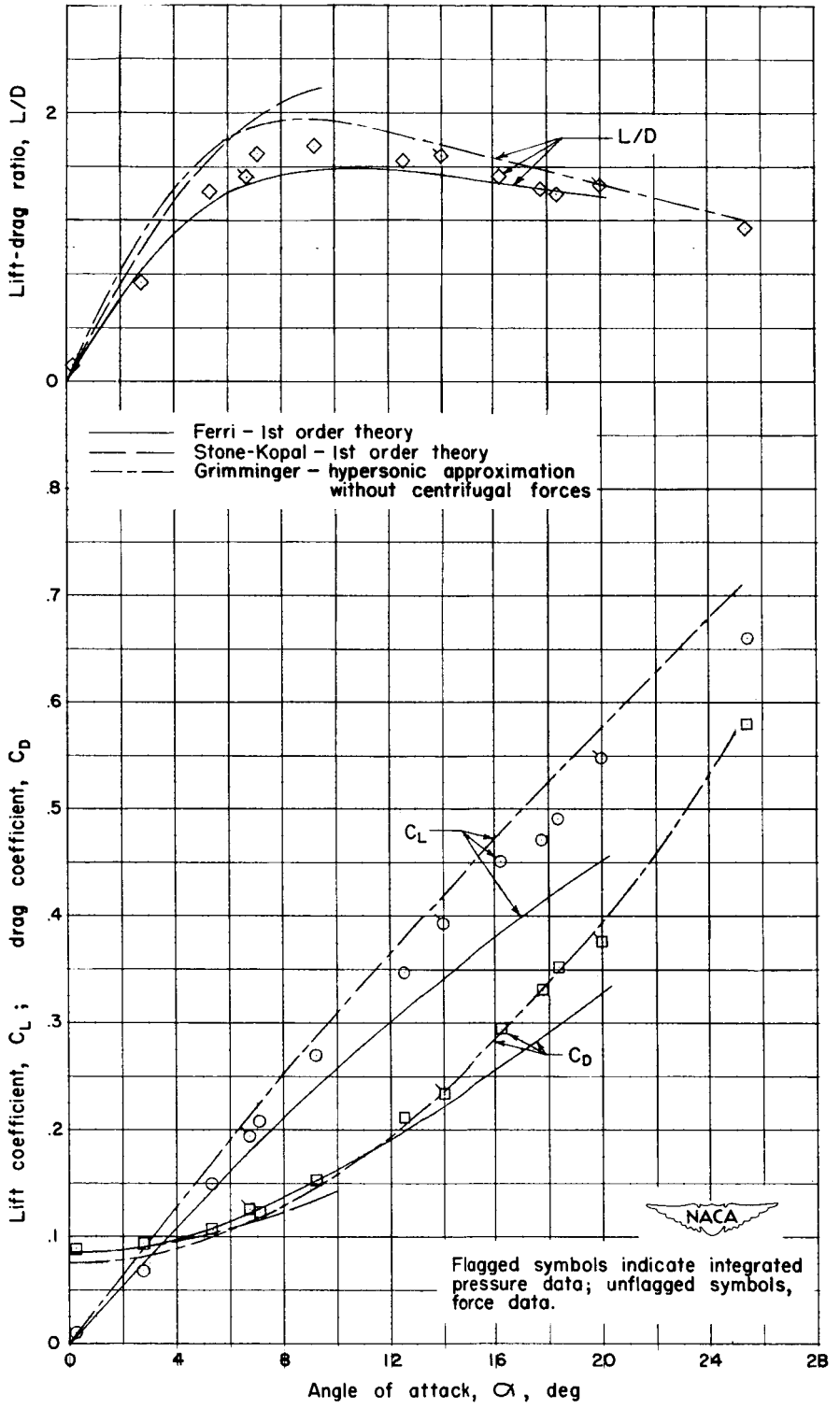

Figure 10.- Variation with angle of attack of the aerodynamic characteristics of the 20° cone. M = 6.86.

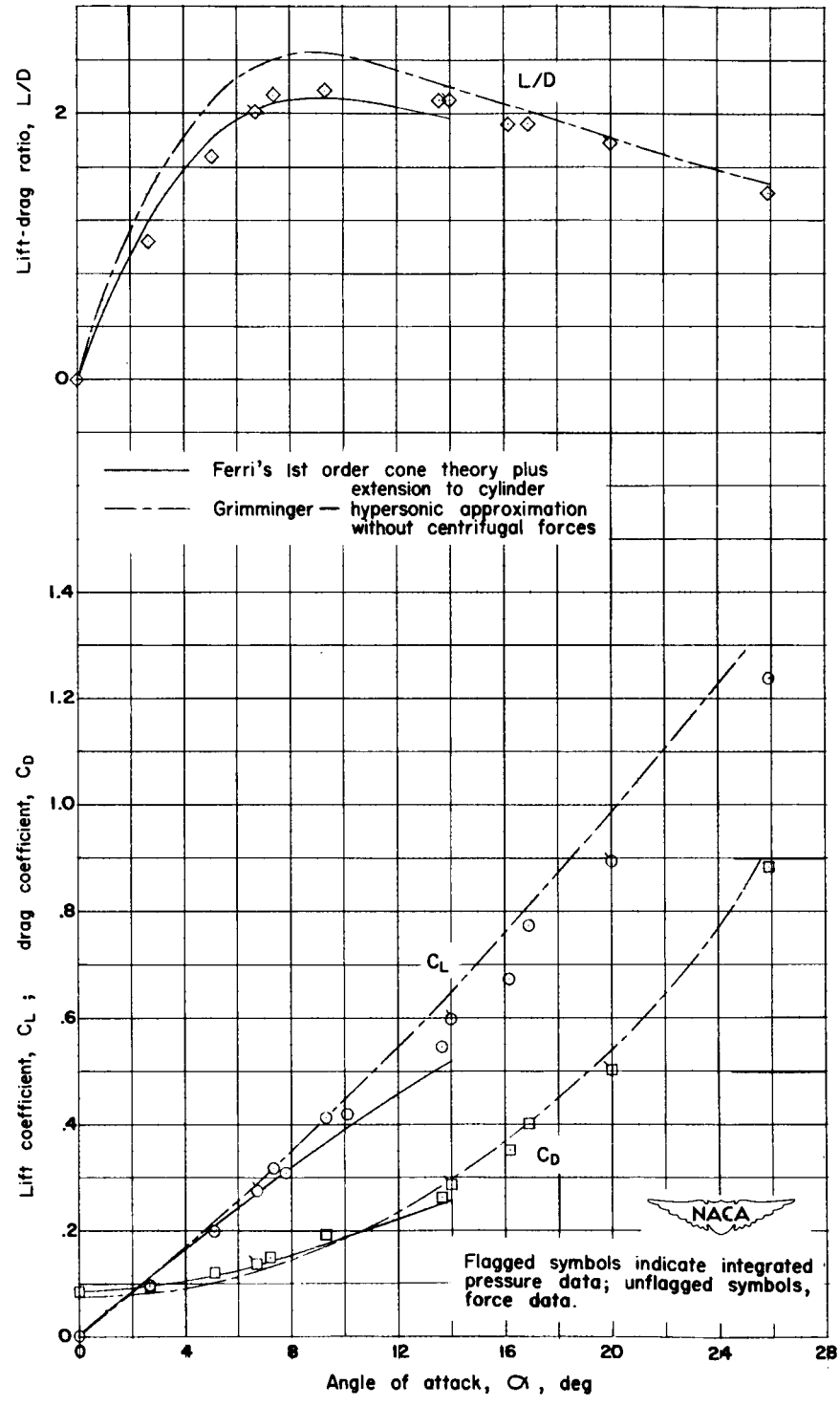

Figure 11.- Variation with angle of attack of the aerodynamic characteristics of the 20° cone cylinder with $\frac{l}{d} = 2$. M = 6.86.

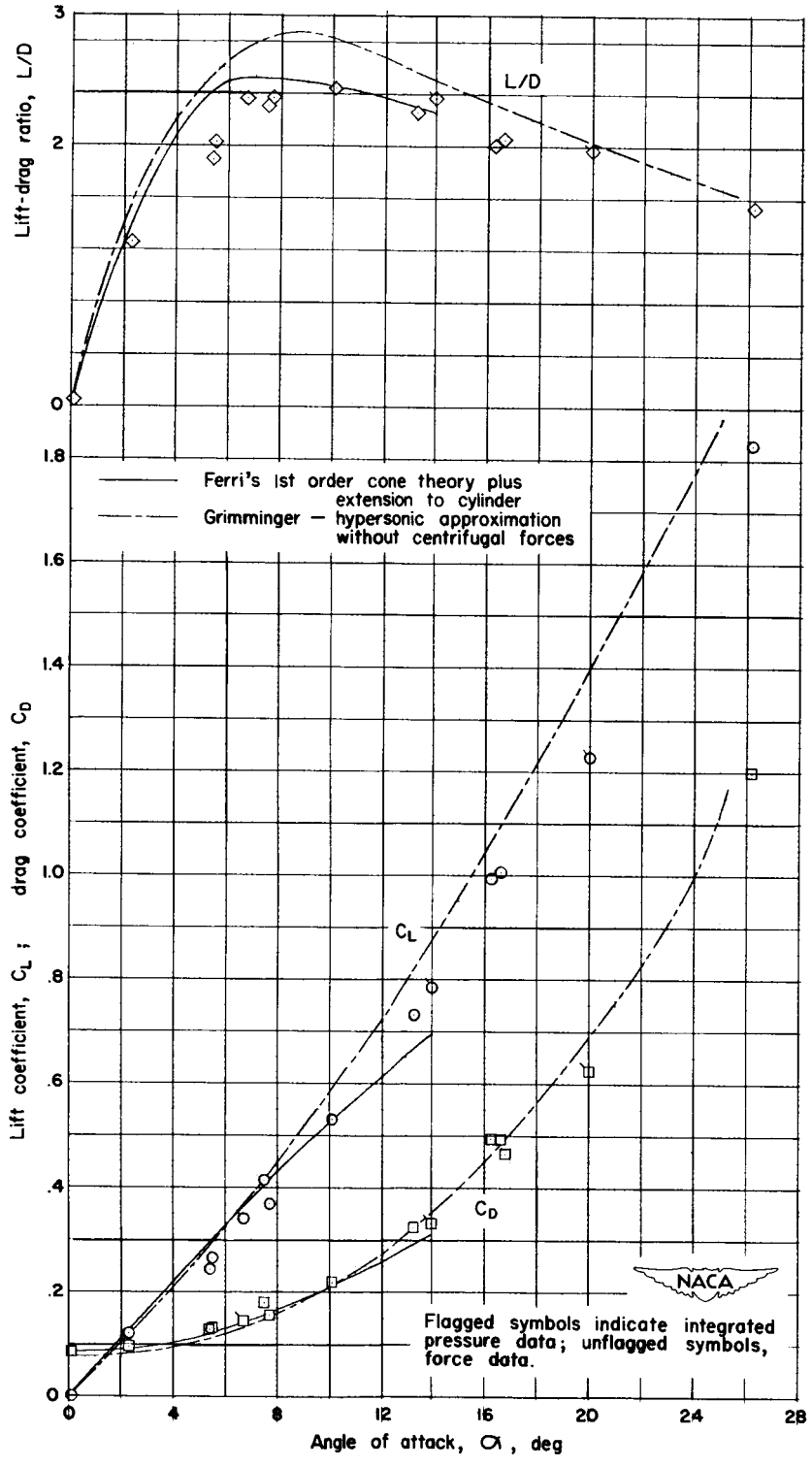

Figure 12.- Variation with angle of attack of the aerodynamic characteristics of the 20° cone cylinder with $\frac{l}{d} = 4$. M = 6.86.

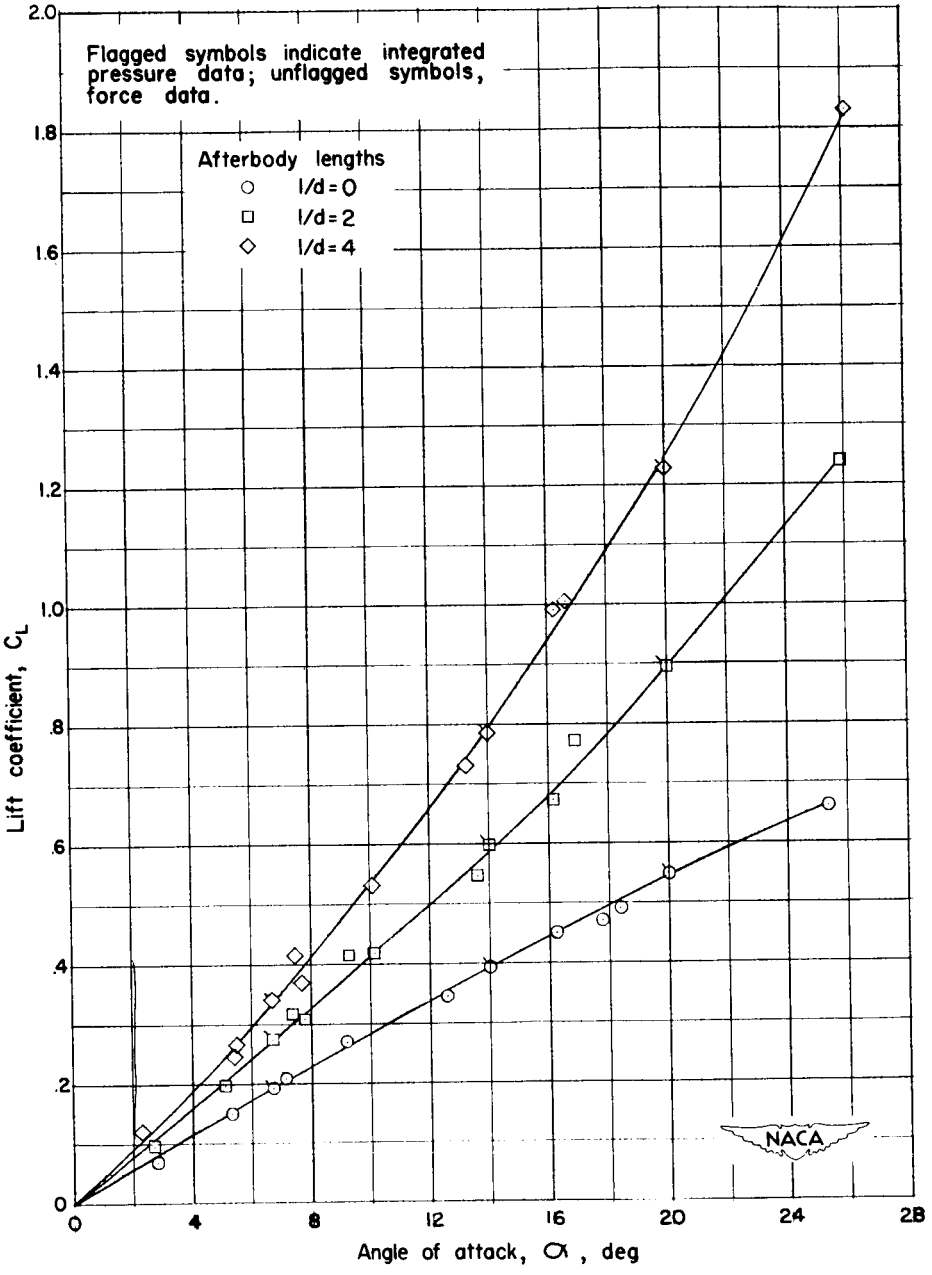

(a) Lift coefficient.

Figure 13.- Comparison of the aerodynamic characteristics of three 20° cone-cylinder configurations having afterbody length-to-diameter ratios of 0, 2, and 4. M = 6.86.

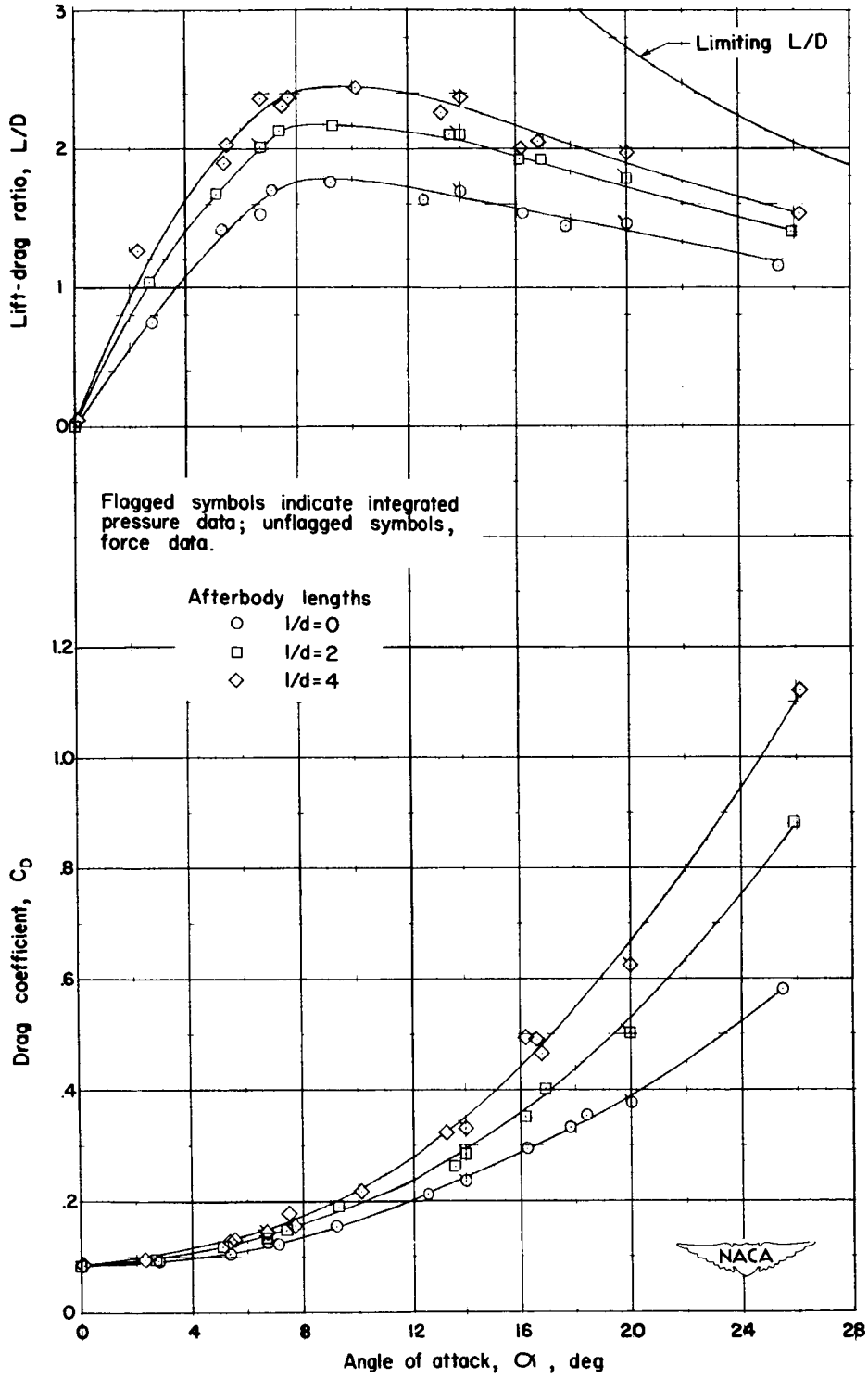

(b) Drag coefficient and lift-drag ratio.

Figure 13.- Continued.

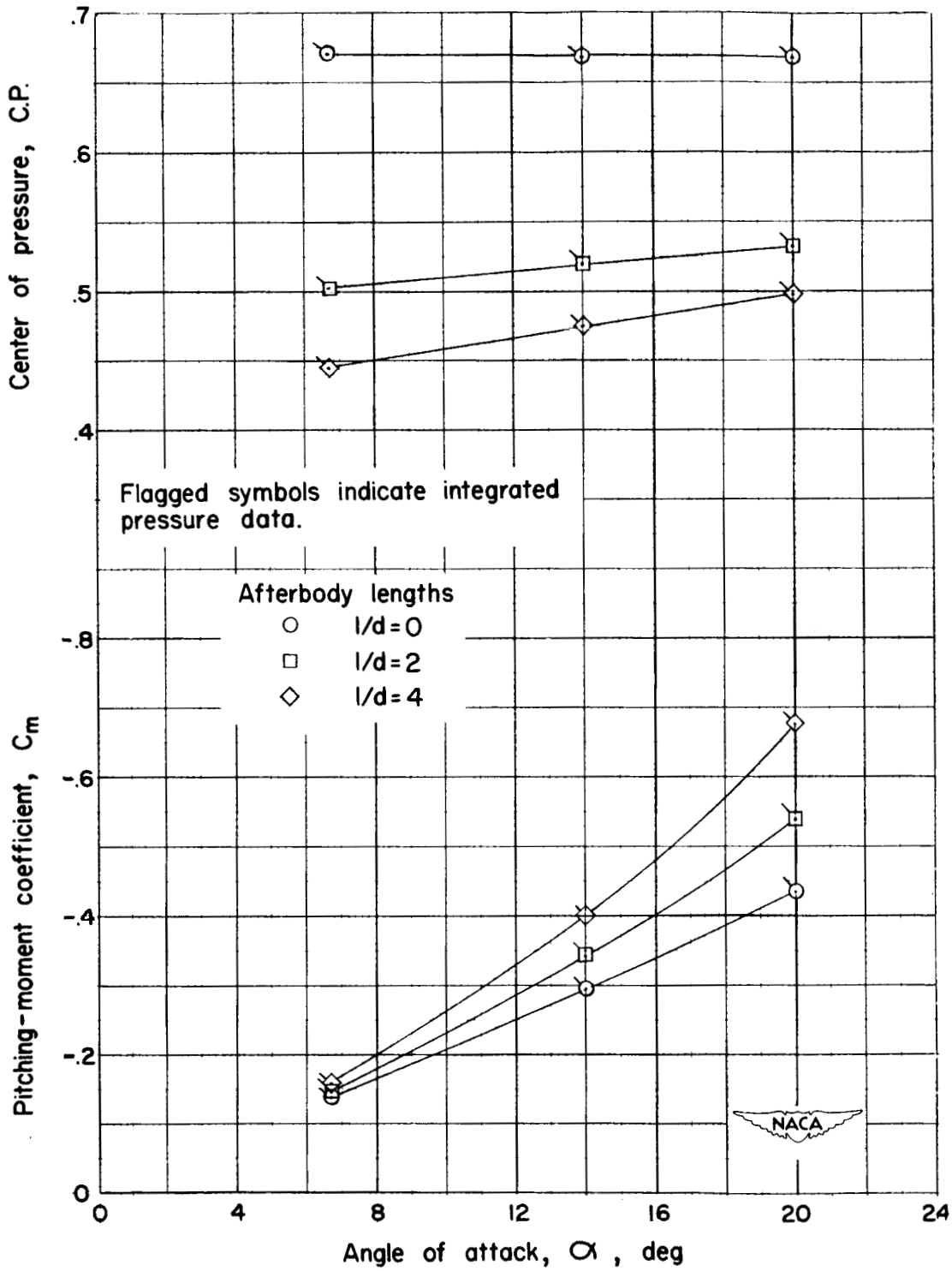

(c) Pitching-moment coefficient and center of pressure.

Figure 13.- Concluded.

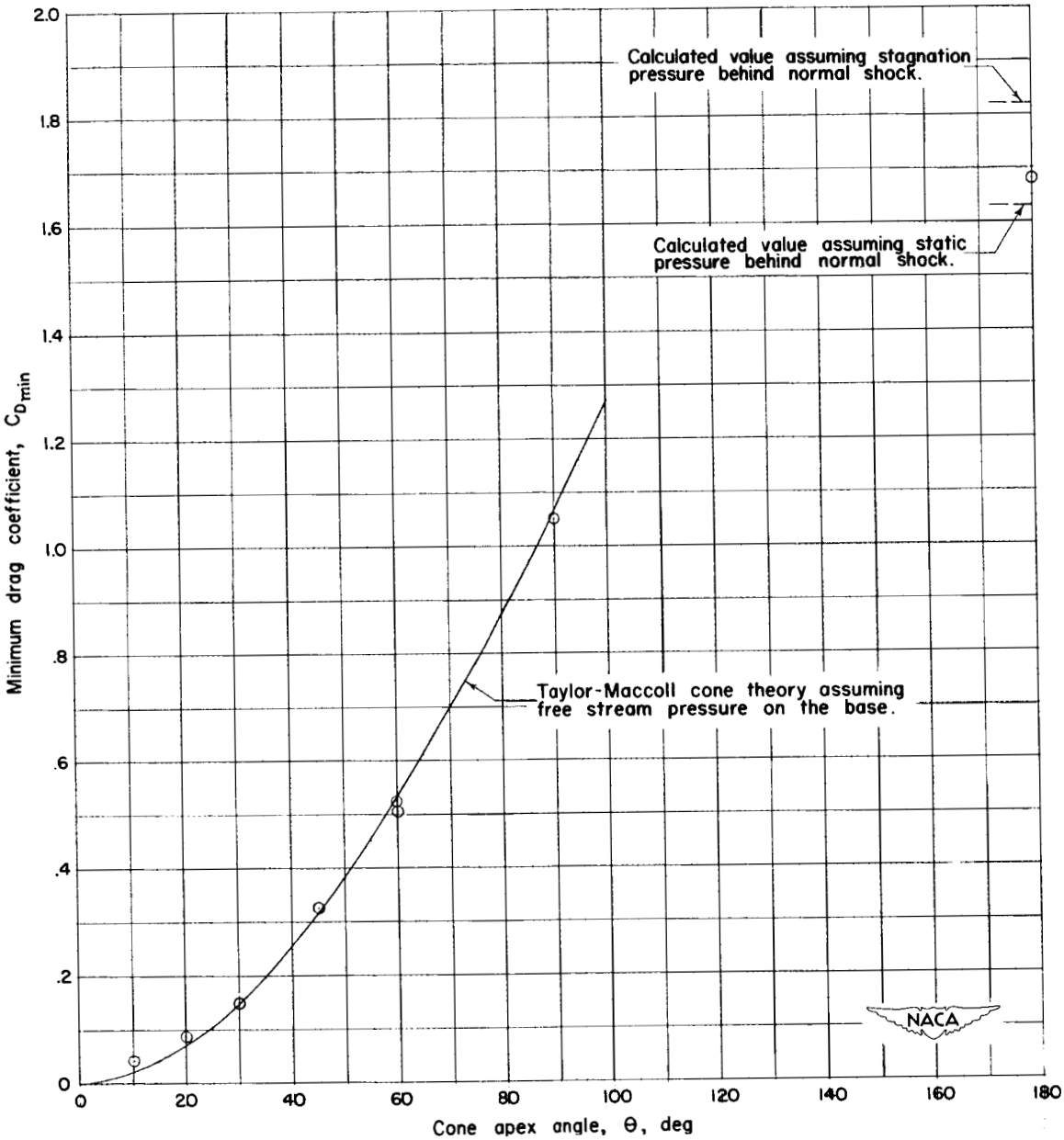

Figure 14.- Variation with cone apex angle of the minimum drag coefficient of the cone-cylinder configurations having $\frac{l}{d} = 4$. M = 6.86.

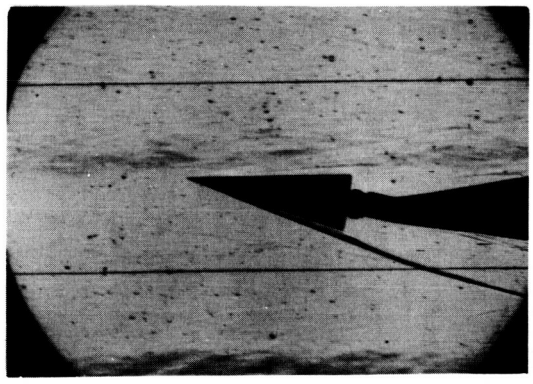

α =9.2°

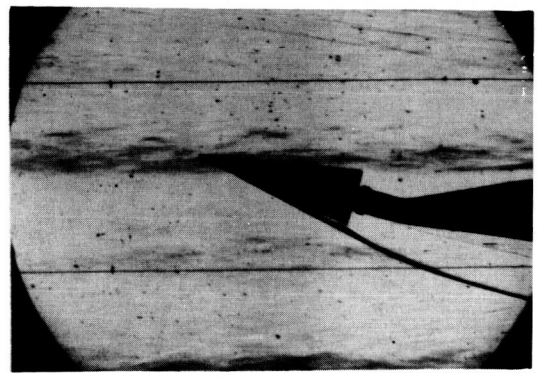

α =16.2°

20° Cone

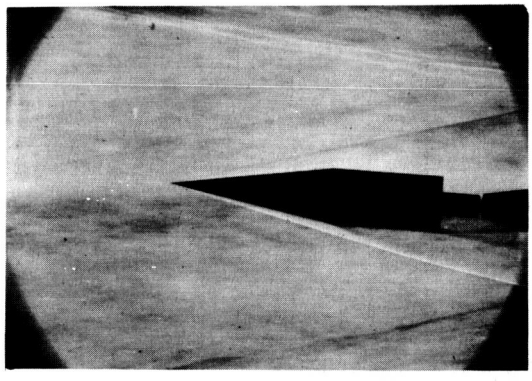

α =5.1°

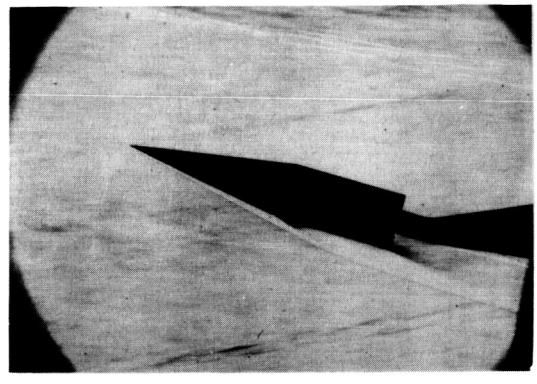

α =16.2°

20° Cone-cylinder, l/d = 2

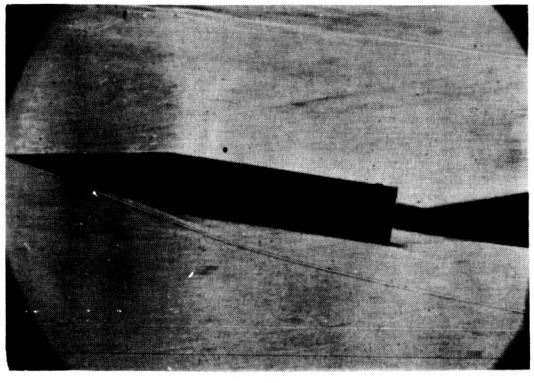

α =10.1°

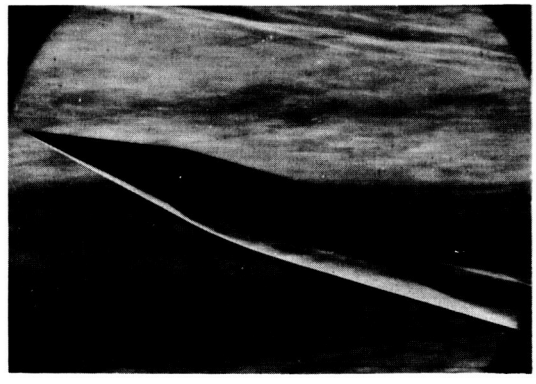

α =16.6°

20° Cone-cylinder, l/d = 4

Figure 15.- Schlieren photographs of the cone and cone-cylinder configurations. M = 6.86.

NACA L-70804

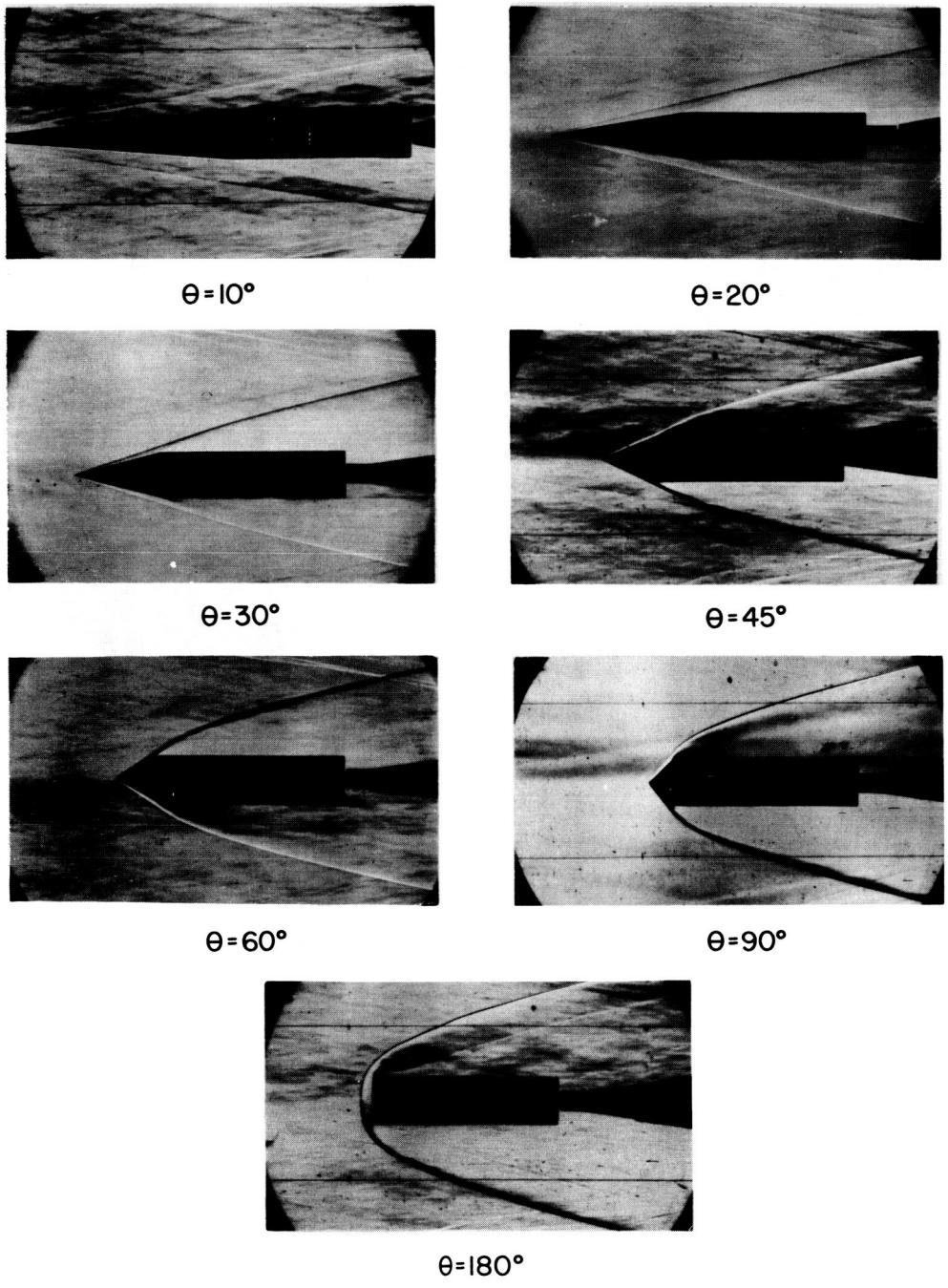

NACA
L-70805

Figure 16.- Schlieren photographs of cone-cylinder configurations with varying apex angles and identical cylindrical afterbodies with $\frac{l}{d} = 4$. M = 6.86.